100,000 years climatic cycles recorded on very high-resolution seismic data from the Santos Basin's upper slope during the last 800 ka

Marina Rabineau, Massinissa Benabdellouahed, Agnès Baltzer, Romain Pellen, Antonio Tadeu dos Reis, Renata Maia, Zohra Mokeddem, Sidonie Revillon, Philippe Schnurle, Karen Costa, et al.

Revised Manuscript submitted to Journal of South American Earth Sciences

100,000 years climatic cycles recorded on very high-resolution seismic data from the Santos Basin's upper slope during the last 800 ka

Marina Rabineau*[1], Massinissa Benabdellouahed[1], Agnes Baltzer[2], Romain Pellen[1], Antonio Tadeu dos Reis[3], Renata Maia[3,7,8], Zohra Mokeddem[1], Sidonie Révillon[4,1], Philippe Schnurle[1], Karen Costa[5], Felipe Toledo[5], Estelle Leroux[1], Maryline Moulin[1], Adriano Roessler Viana[6], Daniel Aslanian[1]

(1) Geo-Ocean, Univ Brest, CNRS, Ifremer, UMR6538, F-29280 Plouzane, France
(2) Laboratoire Géolittomer, CNRS, UMR 6554 LETG, Univ. Nantes, 44312 Nantes cédex 3, France
(3) Faculdade de Oceanografia (FAOC), Universidade Estadual do Rio de Janeiro (UERJ), Brazil.
(4) SEDISOR, 65 Place Nicolas Copernic, 29280 Plouzané, France
(5) Laboratôrio de Paleoceanografia do Atlântico Sul, Instituto Oceanográfico, Universidade de São Paulo (LaPAS/IO-USP), Praça do Oceanográfico, 191, 05580-120, Cidade Universitária, São Paulo, SP, Brazil.
(6) Petrobras, Petrobras Exploration, Rio de Janeiro, Brazil
(7) UFF, Universidade Federal Fluminense, Brazil
(8) now at TotalEnergies,avenue Larribau,F-64000 Pau, France

* Corresponding author: marina.rabineau@univ-brest.fr

Keywords: Seismic Stratigraphy, Sea-level, Climatic cycles, Santos Basin, Brazil

Highlights:

• Sub-bottom profiles from the slope of Santos Basin record Glacial/Interglacial transitions as prominent reflectors
• Reflectors correspond to change from silty clay and sand layers (during glacials) to Marl deposition during interglacial
• The last eight 100,000 years cycles (down to MIS19) are well identified on profiles and cores
• At MIS12, we observe a change in seismic architecture and sedimentation rates corresponding to the mid-Brunhes Event.

Abstract

This study proposes to combine seismic stratigraphic interpretation of very high-resolution sub-bottom chirp profiles acquired along the Santos Basin slope on the Southern Brazilian Margin during the SANBA project to recently published results from five continuous long cores acquired in the Santos Basin (sampling sediments as old as 772 ka with detailed biostratigraphic and chronostratigraphic data). The seismic-core correlation is consistent over the area and shows that 100,000 years cycles' terminations (G/IG transitions, identified on long sediment cores) do correlate to strong seismic reflectors identified regionally on chirp profiles.

In particular, the last eight 100,000 years cycles (down to MIS19) are well-identified throughout the area. Additional higher-resolution sea-level drops or cooling events (e.g., MIS4, MIS7b, MIS9b) can sometimes be distinguished on the chirp profiles but only in areas with sufficiently high sedimentation rates (around 10 cm/ka). At MIS12, we observe a change in seismic architecture with more numerous, more closely spaced seismic reflectors but with smaller amplitudes. According to the available data, this change also corresponds to a change in sedimentation rates (smaller rates before MIS12), which may be related to the mid-Brunhes Transition (at 430 ka) and/or the imprint of 400 ka Milankovitch cycles. Two cores show a specific Nanno Foram Ooze at this transition towards the following Super-interglacial MIS11. This study demonstrates the ability and the reliability of very high-resolution chirp profiles to record continuously the stacking of G/IG climatic cycles on the slope of the Santos Basin despite relatively low subsidence rates on this old passive margin and small direct input from rivers. Therefore, the study points to the continuous feeding of the margin by sediment brought up laterally by currents, most probably mainly Brazilian Current (BC) that follows the shelfbreak down to the South.

1. Introduction

During the Pliocene (starting at 5.3 Ma) and the Quaternary (starting at 2.6 Ma, Gibbard and Head, 2009; Head et al., 2015), sea level variations were primarily related to climatic changes through glacio-eustatic cycles (Lambeck et al., 2002) that had major effects on sedimentary deposits, thus shaping the architecture of continental margins. From the base of Pliocene (5.3 Ma) to the mid-Pleistocene (around 1 Ma) (Figure 1), two major climatic events occurred: (1) the installation of an ice sheet in the northern hemisphere around 2.7 Ma (INHG) that led to sea-level variations (up to 50m) coincident with changes in aridity in Africa for example

(DeMenocal, 2004; Haug et al., 2005); (2) a change of dominant cyclicity from 41 ka to 100 ka during the last circa 1 Ma with sea-level amplitudes reaching more than 100 m. This climatic limit within the Quaternary has been known as the 'Mid-Pleistocene Revolution' (MPR) (e.g., Shackleton and Opdyke, 1973; Shackleton et al., 1990; Bassinot et al., 1994; Berger and Wefer, 1996; Paillard et al., 1996; Howard, 1997; Mudelsee and Stattegger, 1997; Maslin and Ridgwell, 2005; Marino et al., 2009; Zhuo et al., 2015). A major change in sea level amplitudes therefore occurred during the MPR, changing from around 50 m before 1 Ma to around 100 m after 1 Ma (Lowrie, 1986; Liesiecki and Raymo, 2005; Grant et al., 2014). More recent studies described this evolution as the 'Middle-Pleistocene Transition' (MPT) (e.g., Lisiecki and Raymo 2007) or 'Early-Middle-Pleistocene Transition' (EMPT) that more probably spans as a transition from 1.4 Ma to 0.4 Ma (Head and Gibbard, 2015) or 1.2 to 0.6 Ma (PAGES, 2016). However, most authors agree that by 800 ka, the changes in amplitudes were complete so that glacial cycles amplitudes reached 100 m with mostly 100 ka duration (PAGES, 2016). Another third change is described at around 430 ka, the Mid-Brunhes Transition (MBT) or Event (MBE) with an especially strong glacial Marine Isotopic Stage 12 (MIS 12) (and low sea-level) (e.g., Rabineau et al., 2006) together with an especially high sea-level and long and warm following interglacial MIS 11 (e.g., Holden et al., 2011; Martinez-Dios et al., 2021). The origin of modern barrier reefs has also been linked to this MBE: MIS 12–MIS 11 transition with high-amplitude sea-level transgression and long interglacial MIS11 (Droxler et al. 2003, Droxler and Jorry, 2013) that followed the long-term early-middle-Pleistocene sea-level regression.

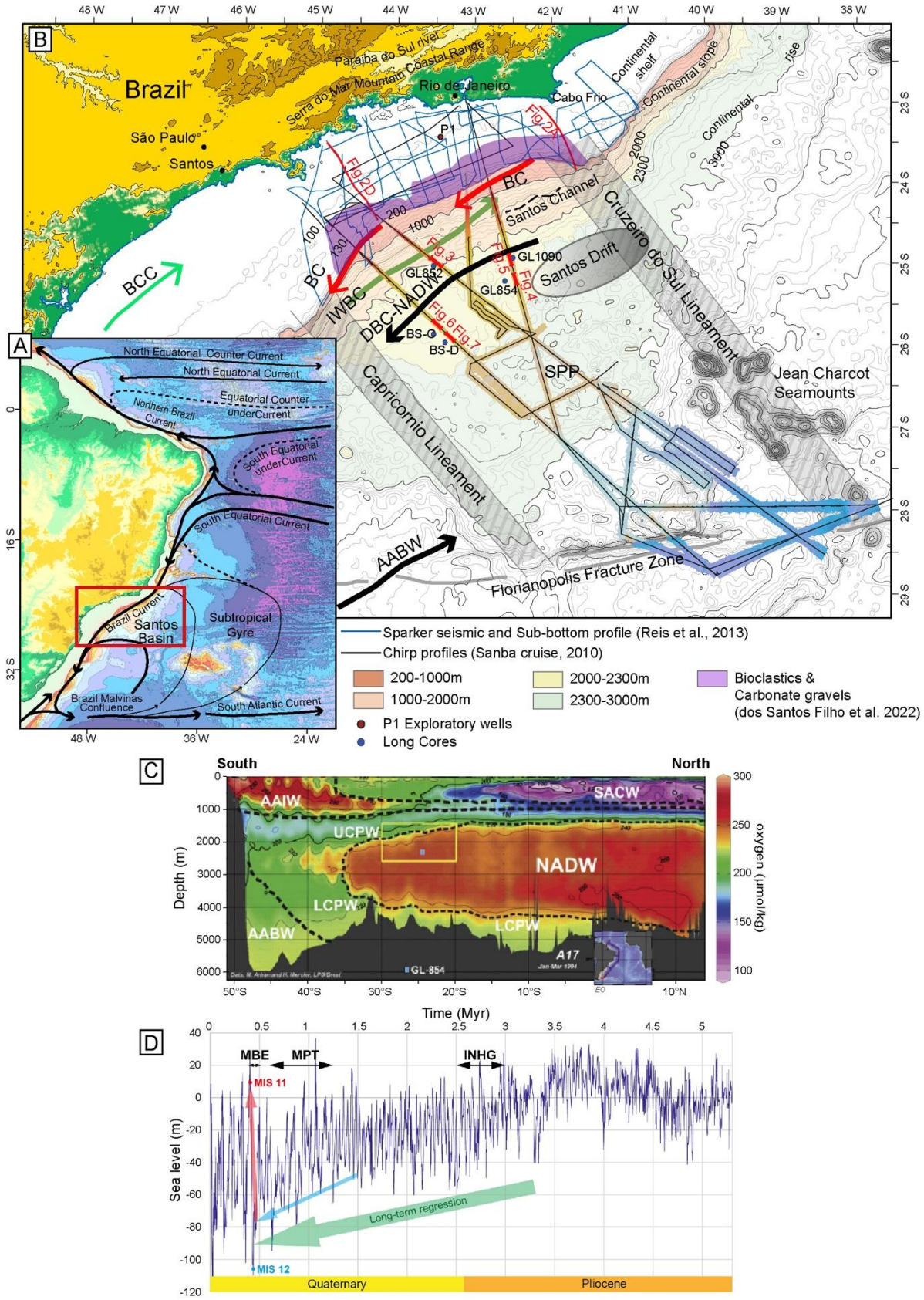

***Figure 1**: (A) Location of the Santos Basin on the Southeast Brazilian margin with schematic major surface currents in South-West Atlantic (Chiessi et al., 2014; Stramma and England, 1999) and estimated bathymetry and global relief from (Smith and Sandwell, 1997) (Mercator projection, WGS84). (B) Bathymetry on the continental slope of the studied area and location of Sub-bottom SANBA cruise profiles acquired in this study (with bathymetry along tracks) and previous existing data on the shelf (Reis et al., 2013) are also shown. Morphology*

map (Mercator projection, WGS84) of the Santos Basin with main fracture zone, lineaments (SPP: São Paulo Plateau), and oceanic currents (BCC: Brazil Coastal Current), which are also shown in (C) oceanic vertical profile from South to North along the Brazilian coast. BC: Brazil Current; AABW: Atlantic Antarctic Bottom Water; NADW: North Atlantic Deep Water; DBC : Deep brazil Current = South Atlantic Central Waters (SACW) + Antartic Intermediate Water (AAIW) + (NADW) (Duarte and Viana, 2007; Lima et al., 2009). Note the position of core GL-854 with the small blue square (D) Sea level variations during the Pliocene and Quaternary (Miller et al., 2020) with the main climatic event. INHG: Initiation of Norther Hemisphere Glaciations, MPT: Mid-Pleistocene Transition; MBE : Mid Brunhes Event; MIS Marine Isotopic Stage.

The relationship between Late Quaternary margins' stratigraphy and sea level changes is well-documented from high resolution seismic data over the world, especially for the last few 100 kacycles (e.g., Kolla et al., 2000; Schuur Duncan et al., 2000; Liu et al., 2004; Rabineau et al., 2005, 2006; Berne et al., 2007; Ridente et al., 2008; Bassetti et al., 2008; Tesson et al., 2010; Le Roy et al., 2014; Lafosse et al., 2018). Several studies have been conducted on the continental shelf of Rio de Janeiro State (e.g., Pinheiro-Moreira et al., 2001; Artusi et al., 2007; Fleming et al., 2009; Maia et al., 2010; Reis et al., 2013) and suggested that the continental shelf of the Santos Basin also offers the opportunity to examine the relationship between the architecture of the Quaternary deposits and the 100 ka glacio-eustatic cycles. However, all these studies focused on the continental shelf and could not describe the evolution of the sedimentary bodies towards the basin. They also had a very limited number of available bio-stratigraphic constraints to date the sequences due to the scarcity of drillings and cores reaching the deeply seated sediments. On the slope, seismic stratigraphic interpretation of the Late Paleogene to Recent sedimentation pattern indicates the presence of the Santos Drift System, composed of several contourite deposits dominated by oceanic circulation (Duarte and Viana, 2007). Modern sedimentation on the Santos Basin slope is a combined response to bottom morphology, the along and cross-isobaths flow associated with meandering of the Brazil Current (BC), seaward transport of coastal water (de Mahiques et al., 2020, 2021a), and deeper currents like the Deep Brazil Current (DBC) (see details in section 2.3 and Figure. 1).
In brief, as stated in Toledo et al. (2016): "*there are few quantitative biostratigraphic studies of chronologically-tuned events or sections in the southwestern Atlantic, and they are time restricted covering a maximum of 130,000 years*". Toledo et al. (2016) offer a review of quantitative calcareous nannofossils and planktonic foraminiferal assemblages compared to high-resolution isotopic record ($\partial^{18}O$) over the last 772 ka from core GL-854 in the Santos Basin. Since 2016, a number of other recent papers have undertaken paleoclimatic studies on long cores that now provide detailed chronostratigraphic constraints (Lessa et al., 2017; Santos et al., 2017; Costa et al., 2018; Camillo et al., 2020). However, **none of those paleoceanographic studies provided any correlation to the sedimentary sequences as**

seen on seismic data. This is the purpose of this paper. We, therefore, focus on our very high-resolution seismic stratigraphy interpretation of sedimentary sequences on the continental slope of the Santos Basin using chirp profiles acquired during the SANBA oceanographic cruise on R/V L'atalante and their correlation with published results from cores (see section 3. Data and methods) to better date and characterize the sequences and their seismic expression.

2. Regional Setting

2.1. Geological background

The Santos Basin is located on the southeastern Brazilian continental margin, between latitudes 29°00'S and 23°00'S (Figure 1). The Santos Basin was part of the East Brazil rift system (e.g., Chang et al., 1992), together with other eastern Brazilian basins, formed during the Jurassic-Early Cretaceous rifting that led to the opening of the South Atlantic Ocean (Rabinowitz and LaBrecque, 1979; Nürnberg and Müller, 1991; Cainelli and Mohriak, 1999; Aslanian et al., 2009; Moulin et al., 2010, 2012).

The Santos Basin is limited by the two NW-SE oriented lineament, the Cruzeiro do Sul Lineament (Gonçales De Souza, 1991), connecting Cabo Frio High with the Jean Charcot seamounts, and the Capricórnio Lineament which separates the Santos Basin of a narrower 270 km-wide sub-basin to the east without any salt layer in the deep domain (Bueno et al., 2004). Toward the south, the Santos Basin is bordered by the Florianópolis High and Florianópolis Fracture Zone (FFZ) (Contreras et al., 2010; Moulin et al., 2012). The FFZ corresponds to one of the most fundamental structures of the formation of the South Atlantic (e.g., Sibuet et al., 1984; Contreras et al., 2010; Moulin et al., 2010). Five major stages characterize Santos basin evolution (Chang et al., 1992; Modica and Brush, 2004; Contreras et al., 2010; Garcia et al., 2012;): pre-rift (Jurassic to Berriasian), syn-rift (Berriasian/late Barremian), syn-rift sag (late Barremian/late Aptian), post-rift (early-middle Albian), and drift (late Albian to Holocene). The movement of the Aptian evaporite layers controls the sediment morphology from the late Cretaceous to the present especially on the lower slope and deep basin (Carminatti and Scarton, 1991). Subsidence rates vary greatly from syn-rift to post-rift and drift stages. Contreras et al. (2010) defined 6 main trends in subsidence evolution for the south Santos basin, with different values on the shelf, upper-middle slope, lower-slope and deep basin. For the last 10 Ma, these values are around 20-30 m/Ma on the shelf-upper-middle slope (0 to 1,000

m water depth), but reach around 50 m/Ma on the lower slope-deep basin (2,000-4,000 m) (Contreras et al., 2010).

2.2. Morphological, hydrological, and sediment source context

The Santos Basin, located in Southeastern Brazil (Figure 1), displays a long coastal mountain range called Serra do Mar. The coastal system, is characterized by the absence of large rivers, a series of large bays and several islands constituted by Precambrian rocks (Milliman, 1978; Zalan and de Oliveira, 2005). The shelf progradation during the late Cretaceous and notably during the Paleogene is known to be linked to the occurrence of high rates of clastic influx coming from an ancestral Paraíba do Sul River that was discharging at that time into the northern Santos Basin (Modica and Brush, 2004). However, at least since the Late Cretaceous, the Serra do Mar also started to be created by uplift (Almeida et al., 2017). This is consistent with the Neogene exhumation rates up to 100 m/Ma based on the thermochronological data from both horsts (the coastal Serra do Mar, and the Serra da Mantiqueira, inland) (Cogné et al., 2011, 2012; Salgado et al., 2016). The ancestral Paraíba do Sul River was captured and diverted inland and to the South (Schattner and de Mahiques, 2021). As a consequence, the shelf environment was drowned and became relatively starved of direct strong input from the continent. The lack of significant direct river input is also counterbalanced by the existence of the Brazil Coastal Current (Figure 1), which brings some terrigenous sediments from the Rio de la Plata to the middle-outer shelf in this area (Souza and Robinson, 2004; Nagai et al., 2014; de Mahiques et al., 2020). The transport and deposition in the Santos basin is therefore controlled primarily by along-margin ocean currents (Schattner et al., 2020; de Mahiques et al., 2020) (see next paragraph). Modern sedimentation on the slope are mostly dominated by lithoclastic sediments and the presence of mid-outer shelf mud depocenters (Ferreira et al., 2020). Sedimentation rates have been measured recently on the shelf and upper slope using radiometric methods and showed variations from 0.49 to 3.73 $cm.yr^{-1}$ in cores with 3 sectors identification (North, South and Central) with varying influence (Ferreira et al., 2020). The central sector, which is our zone of interest, showed weaker influence of the BCC, and a primary source of sediment from Precambrian terrains as shown by geochemical analysis (Nd and Pb radiogenic isotopes). These sediments are being transported from rivers located northward and secondarily by small drainage systems from the Serra do Mar (de Mahiques et al., 2021).

The Santos Basin has been classically regarded as a sediment starved sediment margin since the Oligocene (Modica and Brush, 2004). However, the Neogene-Quaternary sedimentary succession of the Santos Basin shelf-slope environments has not been a subject of considerable attention. Actually, a few studies concerning the Late Quaternary off Rio de Janeiro State (Friederichs et al, 2013; Reis et al., 2013; Reis et al., 2020) revealed the existence of a network of incised valleys that attests to an effective sediment supply from Serra do Mar to the basin during at least the Late Pleistocene. This paleo river system flowing directly into the shelf can be connected to small drainage basins (like Macacú, Caceribu, and Guandú River systems) that end directly into partially-enclosed coastal environments, like the Guanabara and Sepetiba bays.

2.3 Oceanographic Context

Around 10^{o}S, the South Equatorial Current (SEC) bifurcates and gives rise to the western boundary currents that bath the Brazilian continental margin (Figure 1A and 1C) (Stramma and England, 1999). The North Brazil Current (NBC) and the Brazil Current (BC) form the northern and southern branches of the SEC. The Brazilian Current (BC) is a barotropic boundary current that concentrates its main flow in the upper 500 m and flows south along the shelf-slope, bringing hot and saline Tropical Water (TW) (T=25.0 °C, S=37.1) at the shallower levels; South Atlantic Central Water (SACW) (T=14.0 °C, S=35.5) at pycnocline levels (Silveira et al. 2001; de Mahiques et al. 2002, 2004; Lourenco et al., 2016) in the Santos Basin (Miranda et al., 1998). The BC flows down to the subtropical Convergence Zone around 35°S (the Brazil-Malvinas Confluence, Figure 1A). There, it merges with the Malvinas Current (flowing North) and separates from the coast (Duarte and Viana, 2007), feeding the subtropical gyre. On the other hand, near the coast, the Brazilian Coastal Current (BCC, Figure 1B) flows to the North and carries the Plata Plume Waters and sediments (Piola et al., 2005; Möller et al., 2008; de Mahiques et al., 2020). According to Garfield (1990), the shelf break marks the limit of the Brazilian Current (BC) around the 200 m isobaths. However, more recent studies describe the main flow of the BC down to 500 m (de Mahiques et al., 2021a). Velocities of more than 3 cm.s^{-1} on the surface and above 1.2 cm.s^{-1} near the bottom were measured (Faugères et al., 1998; Viana et al., 1998). Deeper in the water column, the Deep Brazilian Current (DBC) also flows south with three distinct water masses the SACW (South Atlantic Central Water) (down to about 500-600m), the Antarctic Intermediate Water (AAIW) and the North Atlantic Deep Water (NADW) between 2000-3000 mwd. The NADW flows

between two northflowing branches of the Circumpolar water (i.e., the Upper and Lower Circumpolar Deep Water (UCPW and LCPW, Figure 1). In the open deepest basin, below 3,500 mwd, the Antarctic Bottom Current (AABW) flows northward with a velocity of around 10 $cm.s^{-1}$. Current velocity values reaching 30 $cm.s^{-1}$ have been reported near the Vema channel, south of the FFZ (Hogg et al., 1982).

2.4 Previous Study of Seismic Stratigraphy

Maia et al. (2010) and Reis et al. (2013) have proposed a Pliocene-Quaternary stratigraphic framework for the continental shelf offshore Rio de Janeiro (Figure 2) based on the combined analysis of seismic sparker records, drilled petroleum boreholes (Maia et al., 2010) and high-resolution seismic sub-bottom data (Reis et al., 2013). The stratigraphic architecture of the continental shelf is composed of eight major seismic sequences bounded by angular unconformities S1 to S5 (Maia et al., 2010). These five reflectors, S1 to S5, are erosive and frequently show stepped profiles. Each of these seismic reflectors is a major sequence boundary representing a diachronous erosional period related to important sea-level falls (falling stage System tract FSST) and low-stands (Figure 2), when sub-aerial exposure of the shelf was extensive. These surfaces were reworked during subsequent sea-level rises (i.e., transgression) of the next sequence. These seismic sequences were grouped into two distinct stratigraphic sets (Figure 2) identified as Set I (SqC to SqA) and Set II (Sq1 to Sq5). The youngest sequence, Sq5, covers the entire shelf (with siliciclatic and biogenic constructions built on top of the previous Sq 4). Sq5 corresponds to the transgressive and high-stand stage of a new starting sequence (Reis et al., 2013). Maia et al. (2010) have proposed an age of 440-500 ka (Figure 2) for the last five seismic sequences in Set II, using chronostratigraphic data (nannofossil zoning) from oil exploration wells (named P1, see Figure 1 for location). In other words, S5, S4, S3, S2 and S1 surfaces were correlated respectively to Marine Isotopic Stages: MIS2, MIS6, MIS8, MIS10 and MIS12.

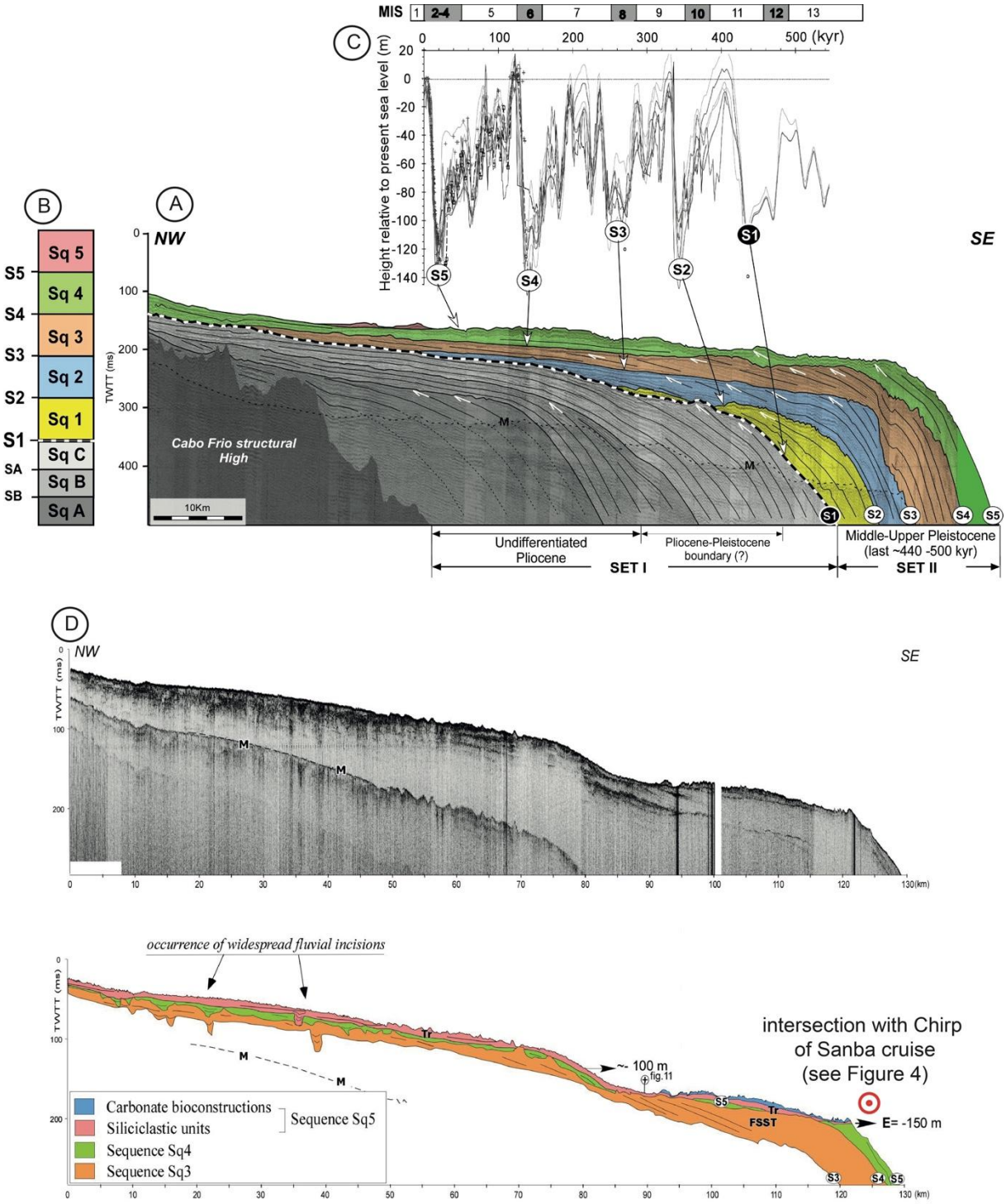

***Figure 2**: (A) Interpreted dip single-channel seismic line (sparker 1000 J) across the eastern shelf sector off Rio de Janeiro State, illustrating a lower aggradational-progradational stratigraphic Set I and Set II ; Set II encompasses Middle-Upper Pleistocene deposition: last ~440-500 Kyr (Maia et al., 2010; Reis et al., 2013) (see position on Figure 1). (B) Sequence boundaries S1 to S5, topping successive 4th order sequences Sq1 to Sq4. Sq5 corresponds to Holocene transgressive and highstand deposition from the current half-cycle (post-LGM). (C) Proposed depositional cyclicity based on correlation with δ18O-derived global sea level variations compiled by (Rabineau et al., 2005). (D) Non Interpreted and interpreted sub-bottom profile acquired on the western shelf sector off Rio de Janeiro (see position on Figure 1) (Reis et al., 2013).*

3. Material and methods

3.1. SANBA cruise (2010)

The SANBA (SANtos BAsin) experiment was a joint project between the Laboratory of Geophysics and Geodynamics of IFREMER (Institut Français de Recherche pour l'Exploitation de la MER, France), the "Géosciences Océan" Laboratory of IUEM (Institut Universitaire et Européen de la Mer, France), the University of Lisbon's Faculty of Sciences (IDL, Portugal), the University of Brasilia (Brazil) and Petrobras (Brazil). The cruise took place in December 2010 (Aslanian et al., 2010a and 2010b). During the SANBA cruise, six multi-channel and wide-angle seismic profiles were acquired in order to image the deep structure of the Santos Basin-São Paulo Plateau System (SSPS) (Evain et al., 2015; Klingelhoefer et al., 2015). Bathymetry and reflectivity data were obtained using a Kongsberg EM122 and EM710 multibeam echosounder. Kongsberg EM122 operates at a main frequency of 12 kHz in marine environments in 100 to 10,000 m. The swath bathymetric map was established with a 50 m grid cell size and displays the morphology of the SSPS between 500 - 4,500 m. In addition to the bathymetry and reflectivity data, high-resolution sub-bottom (chirp) data were acquired. The hull-mounted high-resolution sub-bottom profiler of the R/V Atalante emits frequencies between 1.8 and 5.3 kHz, leading to a vertical resolution of ~30 cm. A total of 6,889 km of bathymetry and reflectivity data, and 7,612 km of high-resolution sub-bottom seismic data were acquired during the deployment and the recovery of Ocean Bottom Seismometers (OBS) in specific areas (close to the Tupi drill site, renamed Lula drill, and the Jean Charcot Seamounts). The data were analyzed and interpreted using the "Kingdom Suite" software and integrated into an "ArcGIS 10.2" software.

3.2. Published Data

Published very high-resolution (chirp) profiles acquired in August 2010 during leg 2 of the oceanographic cruise Rio Costa 1, aboard the Brazilian R/V Cruzeiro do Sul, and published (Sparker) data acquired on the shelf in a joint scientific program between the Woods Hole Oceanographic Institute, Brazilian universities, governmental agencies and private companies, were used to try to correlate shelf and slope interpretations (Figures 1 and 2; Reis et al. 2013).

A literature review enabled us to select five long cores located in the central part of the slope of the Santos Basin, on the upper slope of Santos drift, and ideally located nearby our very

high-resolution profiles (Figure 1 and Table 1 for details on cores). All cores were retrieved by Petrobras. KF-18 (Ferreira et al., 2015) corresponds, in fact, to the same location of core GL 854. Cores GL 852 and GL 854 have very detailed plankton biochronology (Toledo et al., 2016), spanning respectively the last 321 ka (MIS 9 to MIS 1) and the last 772 ka (MIS19 to MIS1). Core GL 1090 (Lessa et al., 2017; Santos et al., 2017) shows a maximum age of 185 ka (MIS6). Cores BS-C and BS-D (Ferreira et al., 2012; Costa et al., 2018) reach respectively ages of 679 and 568 ka (Figure 1 and Table 1). All cores showed detailed and published Age Model and benthic ∂O18 isotopic curves. ∂O18 isotopic curves were measured on *C. Wuellerstorfi* for GL 852, GL 854, BS-C, and BS-D with identified last nineteen MISs (Almeida et al., 2015; Costa et al., 2018 and Toledo et al., 2016). For core GL1090 the benthic ∂O18 isotopic curve was measured using different species *C. Wuellerstorfi* and *Globigerinoides ruber* (Santos et al., 2017). The age models were built by above mentioned authors based on the reference LR04 stack (Lisiecki and Raymo, 2005) using the software Analyseries 2.0 (Paillard et al., 1996).

Core	Lat	Lon	Water depth (m)	Core length (cm)	Max age (ka)	Max MIS	Sed. Rate (cm/ka)	Water depth (in ms twtt)	Core length (ms)	Reference
GL1090	24.92° S	42.51°W	2225	1914	185	MIS6	13	2967	23.92	Santos et al., (2017); Lessa et al., (2017)
GL852	25°01' S	43°33'W	1938	2030	321	MIS9	7.4	2584	25.375	Toledo et al., (2016)
BS-C	25°51' S	43°33'W	2148	2043	679	MIS16	4	2864	25.54	Costa et al., (2018)
BS-D	25°57' S	43°24'W	2171	2121	568	MIS15	4	2895	26.51	Costa et al., (2018)
GL854	25°12' S	42°37'W	2220	2038	772	MIS19	4.3	2960	25.475	Almeida et al., (2015) Toledo et al., (2016) Camillo et al., (2020)

Table 1*- Position and characteristics of the five long cores used for our core-seismic correlation that have been studied and published (see references in the last column). The conversion from meters to milliseconds has been made using a mean velocity of 1,500 m.s.$^{-1}$ in the water and 1,600 m.s.$^{-1}$ in the sediments.*

Additional information was available for four key cores: GL-852, GL 854, BS-C and BS-D, with lithologic Logs (facies identification) and Magnetic Susceptibility measurements (SI) that were done by Petrobras. % CaCO3 curves were measured at South Atlantic Paleoceanography Laboratory at Oceanographic Institute-Sao Paulo University-IOUSP, and were available for cores GL-852 and GL-854. Lithologies spanned from Nanno-Foram Ooze (> 60% CaCO3), Marl (30-60% CaCO3), Carbonate Rich mud (18-30% CaCO3) to Carbonate poor Mud (5-18% CaCO3). Additionally, thin layers of Mixed Sand (with still 18-60%

CaCO3) were described in Cores BS-C and BS-D, and one Mass Transport Deposit (MTD) in core BS-C. See Results section for more information.

3.3. Seismic and cores interpretation

Interpretation of sub-bottom profiles is based on standard seismic stratigraphy methodology (e.g., Mitchum et al.,1977; Catuneanu, 2019) with careful characterization of seismic units according to reflection configurations, seismic facies identification (patterns, frequency, amplitudes) and association with geometries analysis. Seismic discontinuities are described between units with configurations of upper and lower boundaries of units and followed from one profile to another.

For the cores: the published interpretation of isotopic curves from the five available cores (Table 1) were digitized and converted from age (ka) to depth (cm in the core) using the published Age Model, and from depth (cm) to a twtt scale (ms) using a simple average velocity of 1,600 $m.s^{-1}$ in the sediments. This value is a common value observed and measured in many surficial sediments (less than 50 m) on the upper slope all around the world (e.g., Rodriguez-Suarez, 2005 using geotechnical data from offshore Brazil; Marsset et al., 2012 in the Mediterranean Sea). We then had a direct graphic correlation of isotopic curves and published interpreted glacial/interglacial transitions observed in the cores with the seismic profiles and their key reflectors. Some discrepancies or uncertainty can appear between seismic reflector positions and their correlation with core data, because the cores were not exactly located on the sub-bottom profiles, also because the depth-time conversion was done using a constant velocity of 1,600$m.s^{-1}$ which should probably be better tuned using an increasing law with depth velocity. However, considering the small length of the cores (21.2 m as a maximum), the effect of compaction (and increasing velocities) must remain small.

4. Results

4.1. Seismic stratigraphy on the slope

On the upper slope, up to eight major high amplitude and prominent seismic reflectors from top to bottom (R1, R2, R3, R4, R5, R6, R7 and R8) could be followed over all the SANBA dataset limiting 7 sedimentary units above R8. Those reflectors were correlated from one profile to the other and showed a remarkably continuous and homogeneous character, that allowed an easy 3D correlation in the upper slope and in the lower slope (when salt diapirs per-

turbations were not too intense). Unfortunately, the small number of available profiles did not allow us to build isochron and isochore maps.

Above each of these Ri reflectors, the units show overall transparent facies. The 7 units, separated by the strong reflectors, cover a large part of the study area, each unit has a thickness up to 0.006 s TWT (about 5 m) throughout the Santos Basin slope.

In some cases, the transparent facies can evolve laterally to more stratified facies, especially when moving upslope or in local depressions (within mini-basins in between diapirs structures). Therefore, additional second-order reflectors could also be observed (Figures 3, 4 and 5 between R1 and R2 or between R3 and R4 in the depression area). Those additional reflectors appear when sedimentation rates are higher.

Based on seismic facies only, we can say that the R1 to R8 reflectors correspond to a contrast in impedance related to a probable contrast in lithologies. The transparent facies could be related to homogenous clay deposition, while the R reflectors would correspond to a layer of probably coarser sediment that would generate the impedance contrast on the seismic wave.

4.2. Datation of seismic reflectors with isotopic chronology

As explained in the Method section, the published interpretation of isotopic curves from the five available cores (Table 1) were digitized and converted from age (ka) to depth (cm) to a twtt scale (ms) and plotted directly on our very high-resolution chirp sub-bottom profiles.

•The first core GL852 that went through MIS1 to MIS9 was plotted on the chirp sub-bottom profile Leg1-AT0005-020627 (Figure 3). The reflectors R1, R2, and R3 all corresponded to the end of glacial periods (or the termination, i.e., the transition between glacial and interglacial MIS). Therefore respectively MIS2/MIS1; MIS6/MIS5; MIS8/MIS7. On this example an additional smaller-scale reflector could also be identified and correlated to the end of MIS 4 (a cold sub-stage of the last 100,000 years cycle).

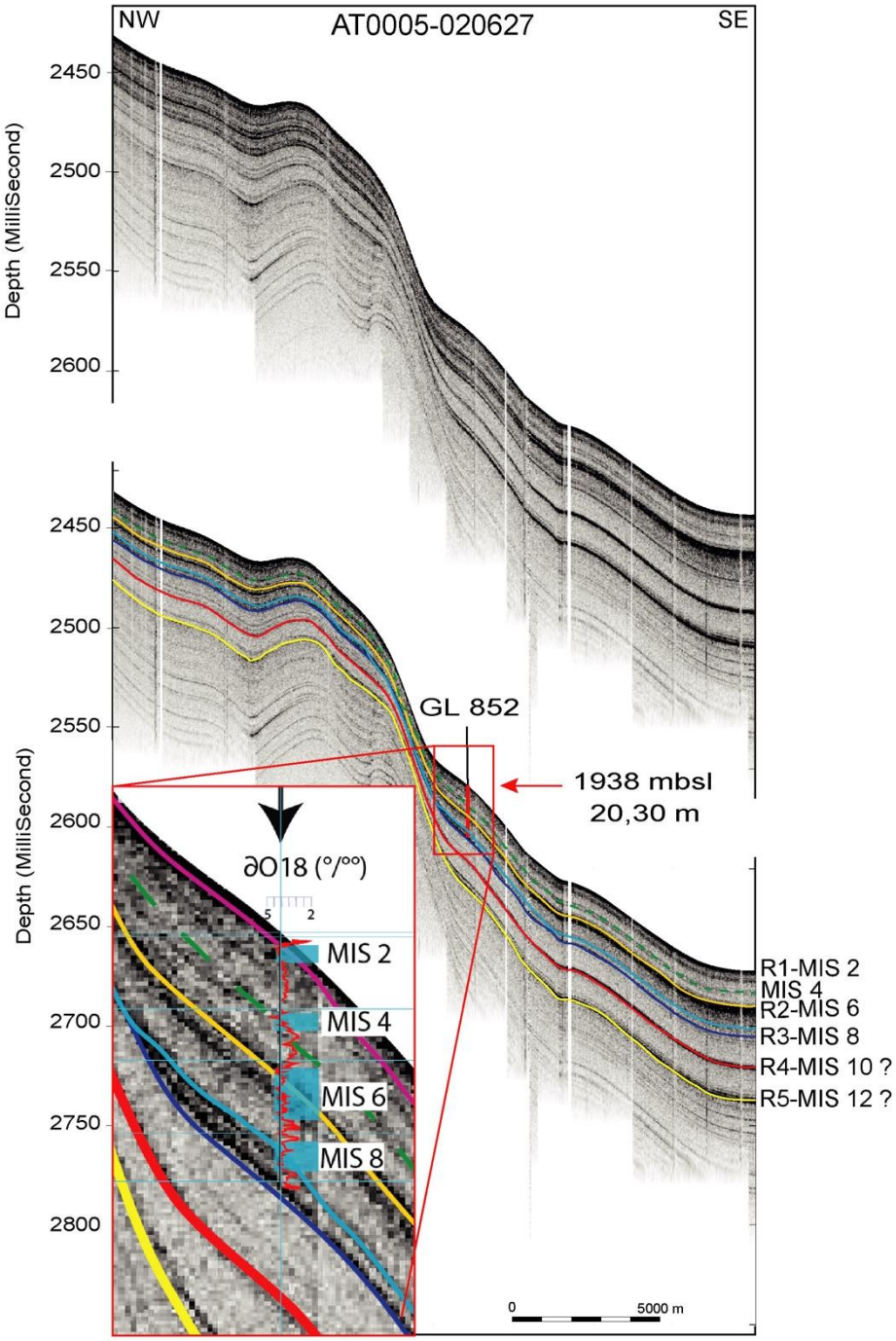

***Figure 3**: Correlation between SANBA Chirp profile AT0005-020627 and core GL 852 (see location on Figure 1). Depth (cm) in core to (ms) transformation was done using a velocity of 1,600 m.s^{-1} in the sediments.*

•The second core GL854 that went through MIS1 to MIS19 was plotted on the chirp sub-bottom profile Leg2-AT0003 (Figure 4). Reflectors R1 to R8 also corresponded to the end of the identified glacial periods or the transition between glacial and interglacial MIS: MIS2/MIS1 to MIS18/MIS17. On the isotopic curves, some other MIS substages were also

identified (e.g., MIS 4 and MIS 9.b). At the position of the core on the seismic, we could not identify other reflectors, but when we move laterally on the profile while following our reflectors, we could identify smaller scale reflectors in between R1 and R2 (that might correlate to MIS4) and also in between R3 and R4 that might correlate to MIS 9b.

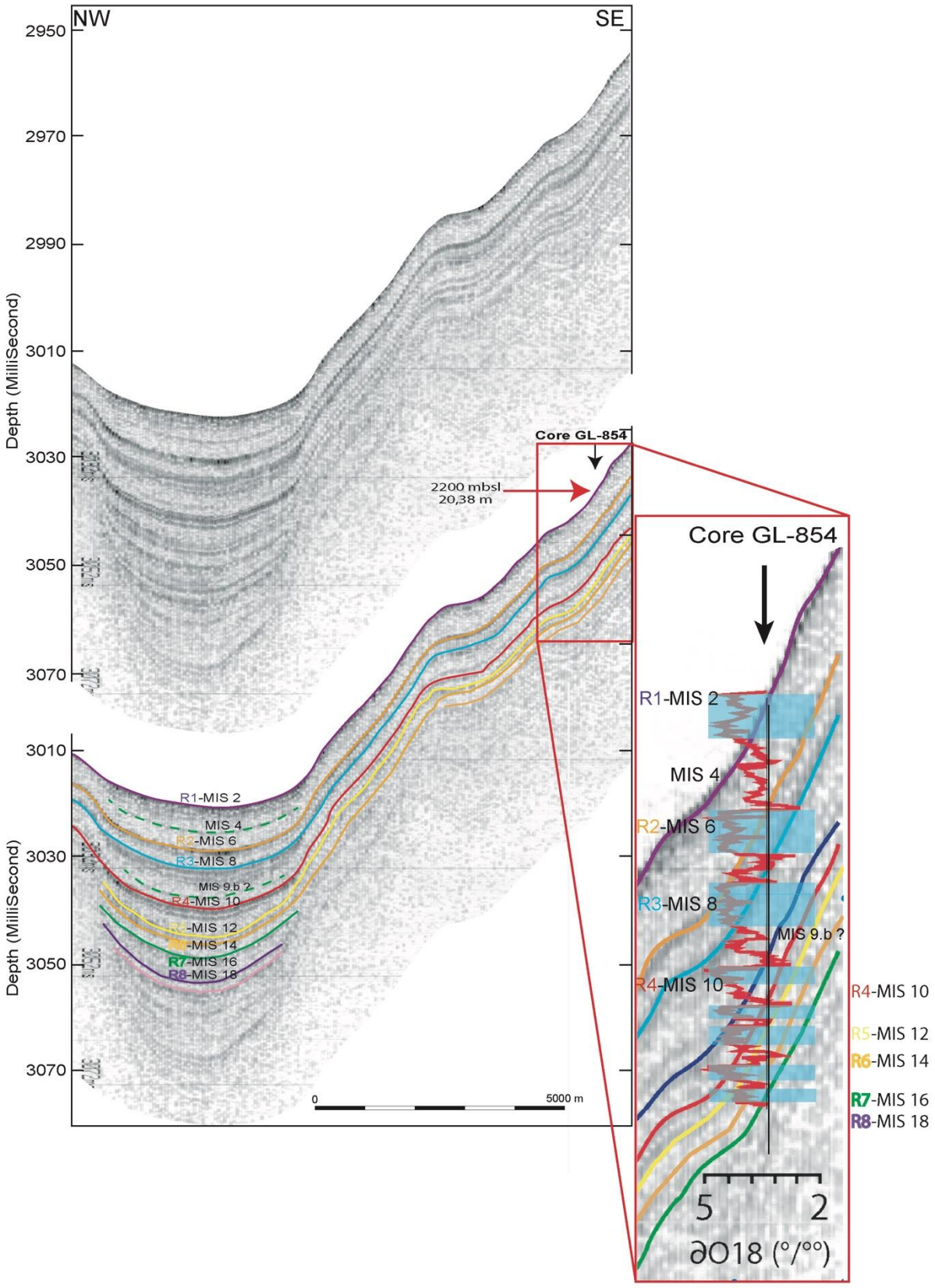

***Figure 4**: Correlation between SANBA Chirp profile AT003 with core GL 854 (see location on Figure 1). Depth (cm) in core to (ms) transformation was done using a velocity of 1,600 m.s^{-1} in the sediments.*

•The third core GL1090 that went through MIS1 to MIS7 was plotted on the chirp sub-bottom profile Leg2-AT0003 (Figure 5). Identified Reflectors R1 and R2 also perfectly correspond to

the position of the end of MIS2 and MIS6, respectively. An additional local reflector was identified between R2 and R1 (Figure 5) and seems to correspond, in this case, to the beginning of MIS4. Note also on this section well-identified reflectors R3, R4, R5 and R6, but that could not be sampled by the too-short core GL-1090.

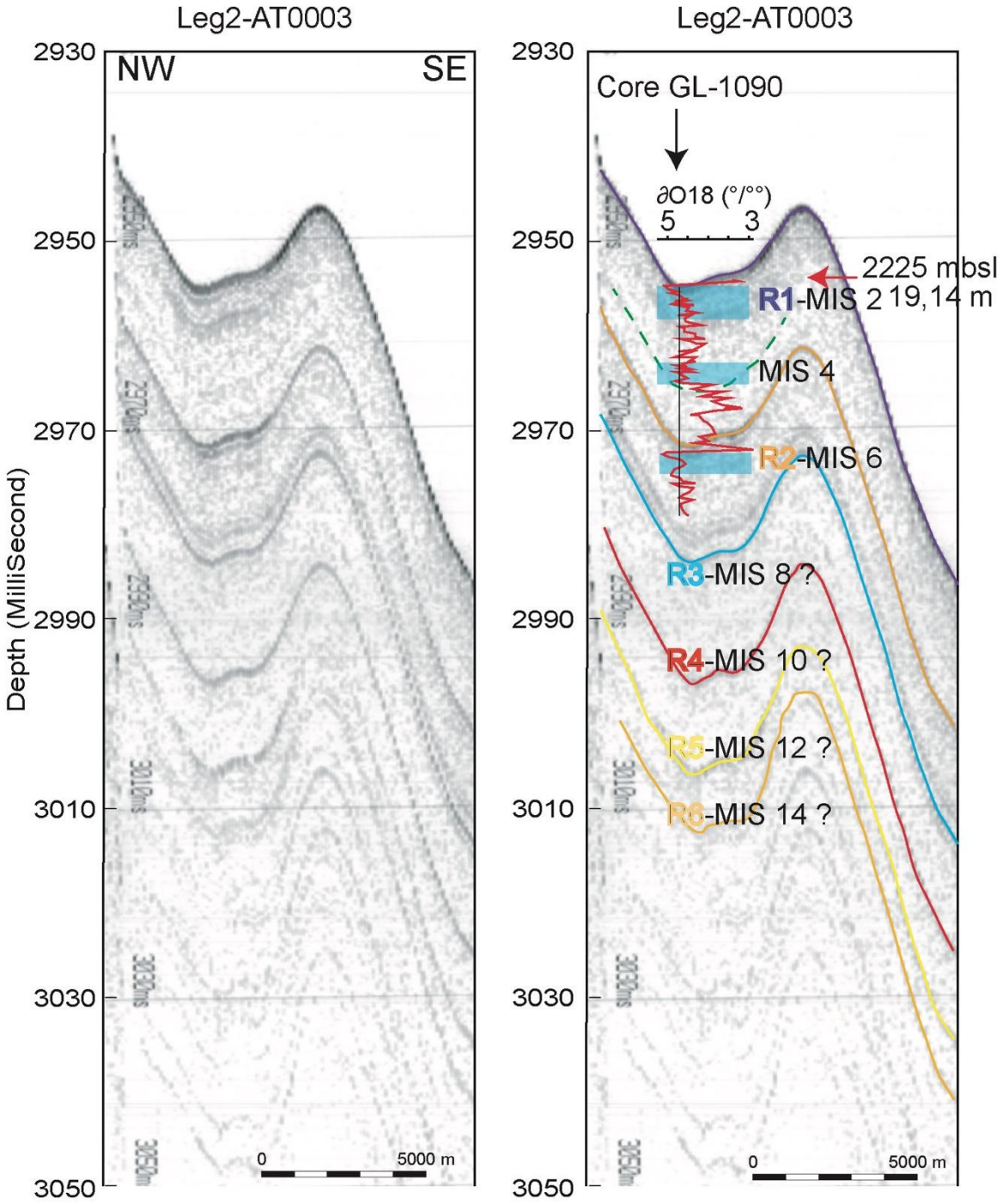

Figure 5: *Correlation between SANBA Chirp profile AT003 with core GL 1090 (see location on Figure 1). Depth (cm) in core to (ms) transformation was done using a velocity of 1,600 m.s^{-1} in the sediments.*

•The fourth core BS-C went through MIS1 to MIS16 and was plotted on chirp sub-bottom profile Leg-AT0016-054719 (Figure 6). Identified reflectors R1 to R5 correspond well to the position of the end of MIS2, MIS6, MIS8, MIS10 and MIS12. In this case, R6 was not so easy to follow. R7 was easier to follow but, in any case, both of them were close to each other, which is also what is seen on the core. Therefore, we associated R6 to MIS14 which is a relatively "smaller" glacial cycle (smaller amplitude and shorter duration) that might explain a less continuous R6 reflector. R7 corresponds to MIS16.

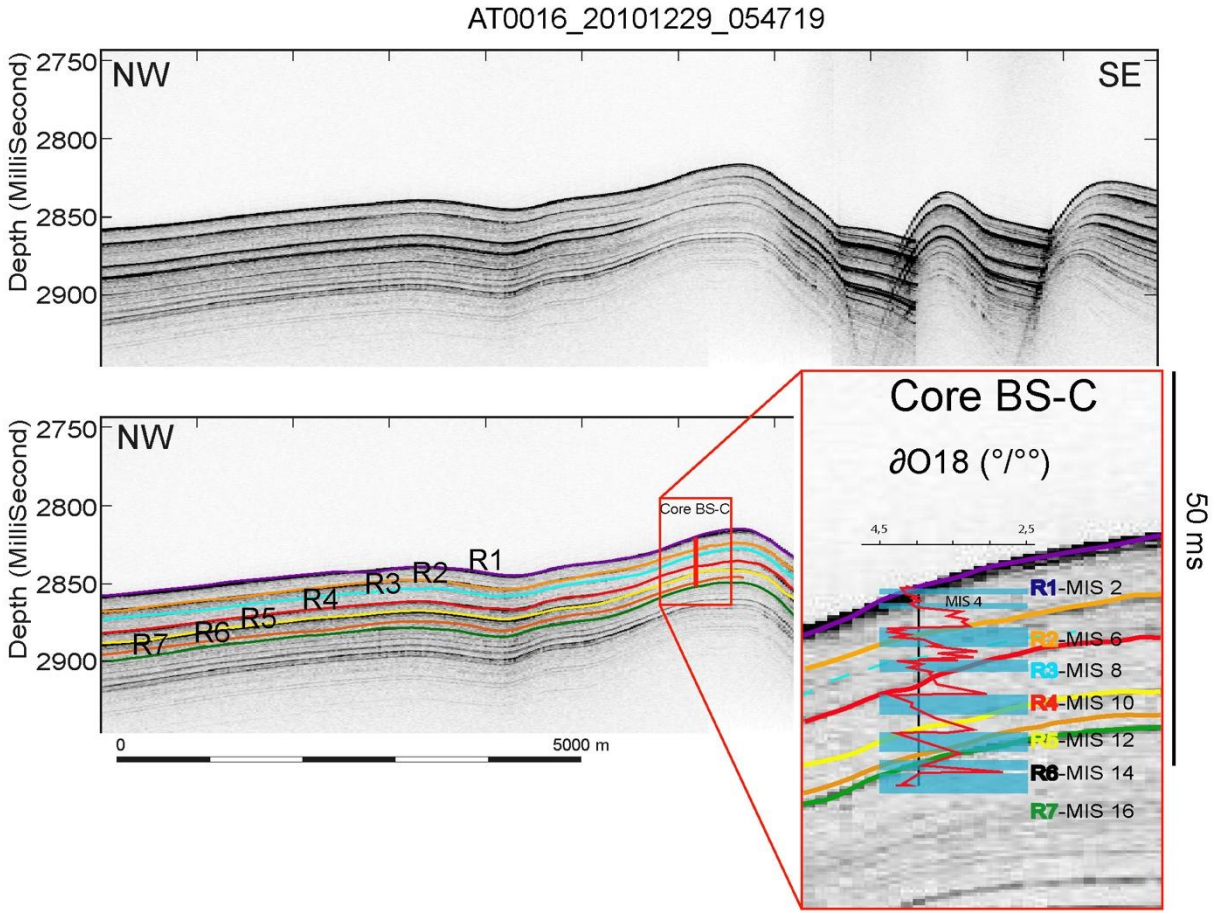

Figure 6: *Correlation between SANBA Chirp profile AT016 with core BS-C (see location on Figure 1). Depth (cm) in core to (ms) transformation was done using a velocity of 1,600 m.s^{-1} in the sediments.*

•The fifth core BS-D that went through MIS1 to MIS14 was plotted on chirp sub-bottom profile Leg2-AT0016-041816 (Figure 7). Identified reflectors R1 to R5 correspond well to the position of the end of MIS2, MIS6, MIS 8, MIS10 and MIS12. Below MIS12, the core seems to have cross through MIS14. However, in this case, R6 was difficult to identify on profile. As stated above, MIS14 is relatively "smaller" glacial cycle (smaller amplitude and shorter duration) that might explain a less continuous R6 reflector.

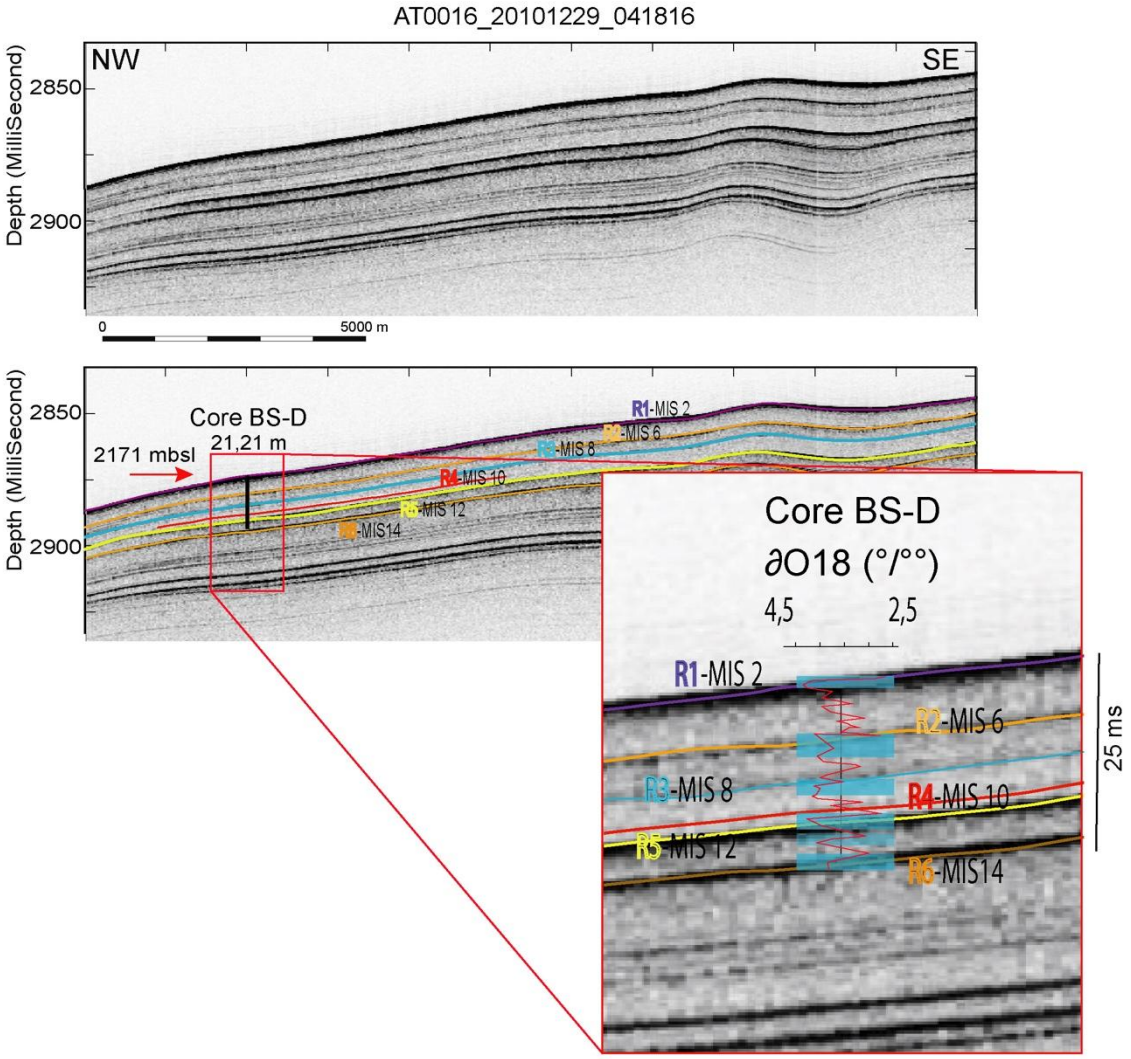

Figure 7: *Correlation between SANBA Chirp profile AT016 with core BS-D (see location on Figure 1). Depth (cm) in core to (ms) transformation was done using a velocity of 1,600 m.s^{-1} in the sediments.*

Therefore, all correlations show a remarkable correlation between Glacial/Interglacial transitions (identified on cores) and the Ri reflectors identified on the seismic (see synthesis in Table 2). R1 corresponds to MIS2/MIS1; R2 to MIS6/MIS5; R3 to MI8/MIS7; R4 to MIS10/MIS11; R5 to MIS12/MIS13; R6 to MIS14/MIS13; R7 to MIS 16/MIS15; R8 to MIS 18/MIS17.

Slope reflector	color	Marine Isotopic stage	Shelf reflector	Maia et al. (2013)	Sed. Rates (cm/kyr) per IG/G cycle (GL854) Almeida et	Mean Sed. Rates (cm/kyr)

					al. (2015)	
		MIS1	Sea-floor			
R1	purple	Top MIS2	Sub-seafloor	S5	5.69	
R2	orange	Top MIS6			3.19	
R3	blue	Top MIS8			4.93	4.1
R4	red	Top MIS10			2.54	
R5	yellow	Top MIS12	Uc1		1.02	
R6	orange	Top MIS14			3.36	
R7	green	Top MIS16			1.53	1.8
R8	violet	Top MIS18			1.25	

Table 2: *Seismic reflectors with colors on the seismic sections, age from the cores, and tentative correlation to previous interpretation on the shelf. In the last two columns, Sedimentation rates have been calculated using data from GL854 (Almeida et al., 2015) for each G/IG cycles, and in the last column for the two groups MIS18-MIS12 and MIS12-MIS2 to show the change in sedimentation rates after MIS12 (MBE).*

4.3. Lithologies

Lithological descriptions from previous studies show the succession of three main types of facies: marl (35-65% $CaCO_3$), carbonate-rich mud (18-30% $CaCO_3$) and carbonate-poor mud (5-18% $CaCO_3$) (Almeida et al., 2015; Camillo et al., 2020 for GL-854). Lithological description for GL-1090 was as follows: "GL-1090 consists mostly of greenish to olive glacial sediments somewhat rich in foraminifera-bearing silty clay. Carbonate-rich Holocene and Last Interglacial sediments are represented by more reddish-brown and whitish clays, respectively" (Santos et al., 2017). Additional data with magnetic susceptibility and siliciclastic grain size measurements are described in Mathias et al. (2021).

The detailed lithologic descriptions of 4 cores (GL 852, GL854, BS-C, and BS-D) are shown in Figures 8 and 9, together with magnetic susceptibility, ∂O18 benthic oxygen isotope curves, and percentage of CaCO3 measurements (when available).

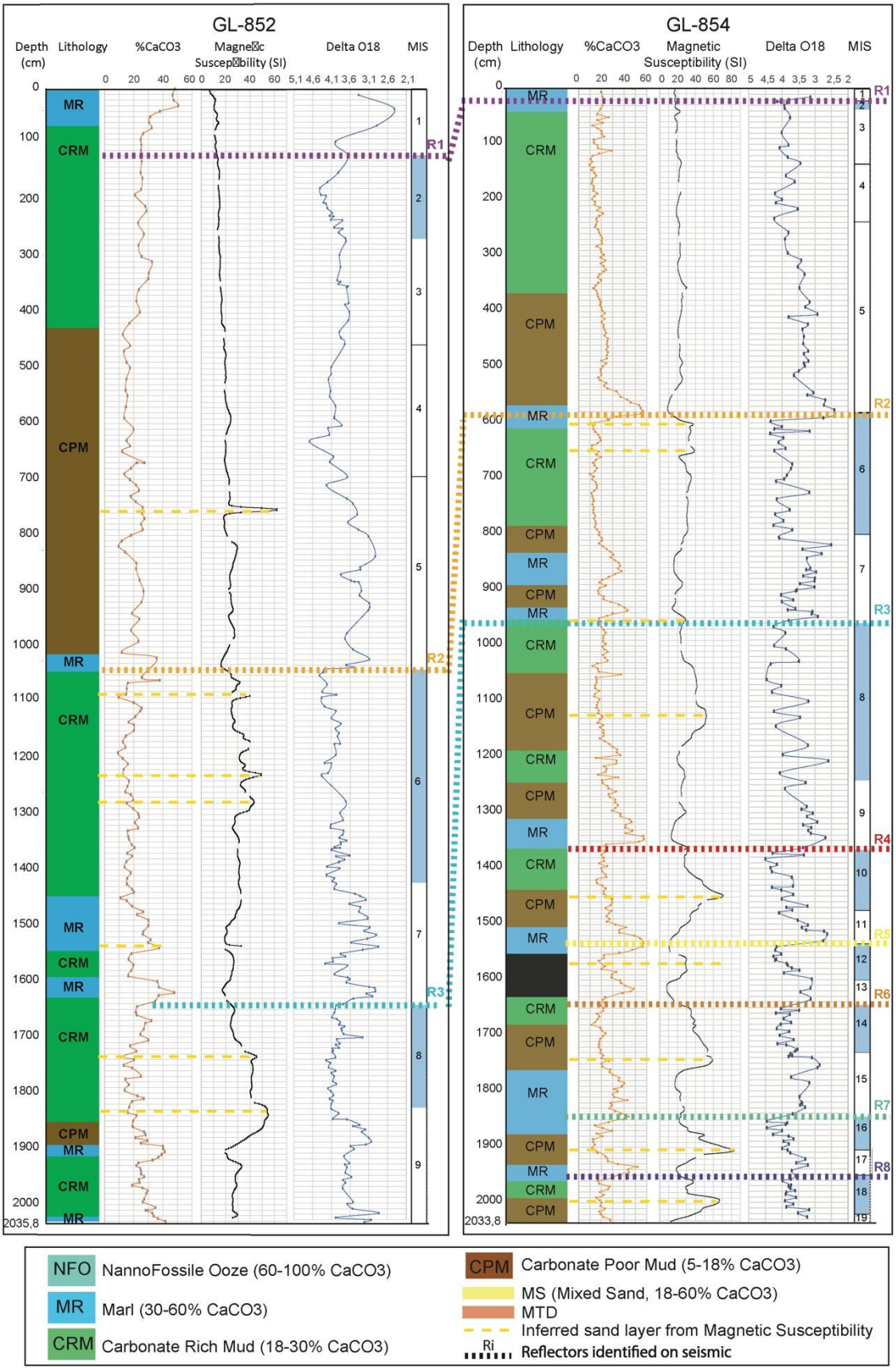

Figure 8: *Description and interpretation of Cores GL852 and GL 854*

The lithologies span Nanno Foram Ooze (> 60% $CaCO_3$), marl (30-60% $CaCO_3$), carbonate-rich mud (18-30% $CaCO_3$) to carbonate-poor mud (5-18% $CaCO_3$). Additionally, thin layers of mixed Sand (with still 18-60% $CaCO_3$) were described in Cores BS-C and BS-D and one Mass Transport Deposit (MTD) in core BS-C.

The position of the Glacial Maxima identified from isotopic curves is shown with blue boxes. The R reflectors (R1 to R8) identified on sub-bottom profiles are also shown on the figures at glacial/interglacial transitions.

Those facies do not appear randomly. In general, the glacial intervals are made by greenish to olive silty clay with a variable amount of Foraminifera. BS-C and BS-D cores also show the existence of Mixed Sand thin layers with a variable amount of $CaCO_3$ between 18-60 %.

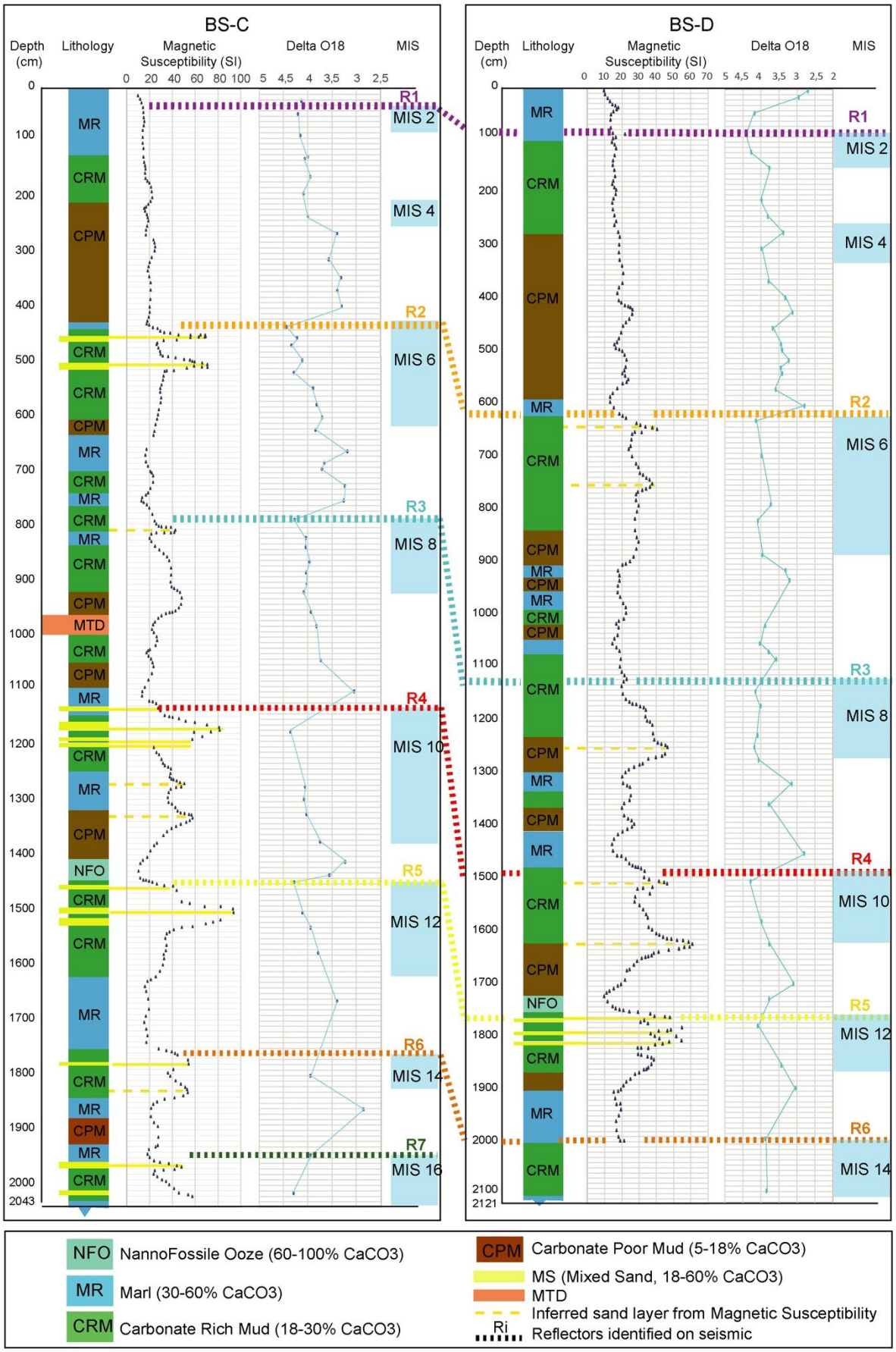

***Figure 9**: Description and interpretation of Cores BS-C and BS-D*

From MIS12 to the present day, each deglaciation (glacial-interglacial transition) is related to a change from silty mud (that tends to be carbonate-rich silty mud during the end of glacial periods) to the deposition of marl (with 35-65% CaCO3) just after the termination. This marl deposition is most often followed by a sequence of carbonate-poor mud (Figure 9). During the glacial periods, lithologies tend to be carbonate-rich mud, but some alternations with carbonate-poor are sometimes described. Before MIS12, the lithological changes do not seem to follow such a regular pattern (Figure 9).

Concerning the thin mixed sand layers described on the sedimentological log, we noticed that they were always associated with a peak of Magnetic Susceptibility (MS). This relationship between magnetic properties of marine sediments is indeed related to sediment composition (e.g., Rothwell, 2006). A high amount of ferro- and paramagnetic minerals will show high magnetic susceptibility whilst biogenic material will show low or even negative values. This is clearly shown in cores BS-C and BS-D, with low MS values for the described Nanno-Foram Ooze and high values for the Mixed Sand layers (Figure 9). Magnetic susceptibility peaks have often been associated with grain size changes in the literature (e.g., Evans and Heller, 2003; Kim et al., 2018) and interpreted as a terrigenous material and possible turbidites indicators (Rothwell, 2006).

We therefore suggest further interpretation of the MS curves to identify "potential" other thin Mixed Sand layers shown in Figures 8 and 9 with dotted orange layers, but that were not described on the sedimentological Log.

We also analyze that those mixed sand layers or inferred sand layers are, in most cases, occurring during glacial Maxima. In BS-C, this is clearly the case for MIS6, MIS10, MIS12, MIS14 and MIS16. In BS-D, this is clearly the case for MIS6, MIS10, and MIS12. For GL-852, we suggest inferred sand layers during MIS6 and MIS 8. In GL-854, we suggest inferred sand layers during MIS6, MIS8, MIS10, MIS12, MIS16 and MIS18.

In core BS-C, a Mass Transport Deposit (MTD) is also observed around 10m within the third Sequence (between R4 and R3) and shows some possible reworking and sliding on the slope. However, this facies, was only observed once in this core.

Finally, both cores BS-C and BS-D show a clearly identified 36cm thick Nano-Foram Ooze just after MIS12, corresponding to the interglacial MIS 11.

4.4. Sedimentation rates

The average sedimentation rates for each core are shown in Table 1. They vary on average between 4 to 13 cm/kyr. Note that those rates are much higher than present-day sedimentation rates recently quantified, using natural radionuclides, on the shelf and outer slope that ranges between 0.49-3.73 cm/kyr (Ferreira et al., 2020). The values for the most distal samples (at water depths between 250 and 540m) are around 1-2 cm/kyr. Previous records that studied post-LGM spanning box cores showed sedimentation rates between 0.5 to 18.4 cm/kyr that are controlled by the shelf and upper slope morphology, the Brazil Current meander dynamics, and the Coastal Water offshore motion (de Mahiques et al., 2002).

The values for post-LGM sedimentation rates in the cores we used are in the lower range (around 5; Table 2). However, note that the cores we use in this study are located much deeper than those of Ferreira et al., 2020 and de Mahiques et al. (2002) (max. depth 1,226 m), with our cores ranging between 1,938 m and 2,225 m depth. Another point of interest is that the cores spanning the longest period of time show the smallest sedimentation rates (around 4 cm/kyr) for GL854, BS-C and BC-D. Based on results published by Almeida et al.(2015), we calculated the average of sedimentation rates per interglacial/glacial cycles based on their table 2 for GL-854. These calculations are shown on our Table 2. Sedimentation rates in GL854 show two main contrasting periods. From the base of cores to top-MIS12, they show smaller sedimentation rates: less than 2 cm/ka; whereas from top-MIS12 (start of MIS11) to present day sedimentation rates show a 2 fold increase (x2), with rates reaching 4 cm/kyr (Table 2 and Figure 10).

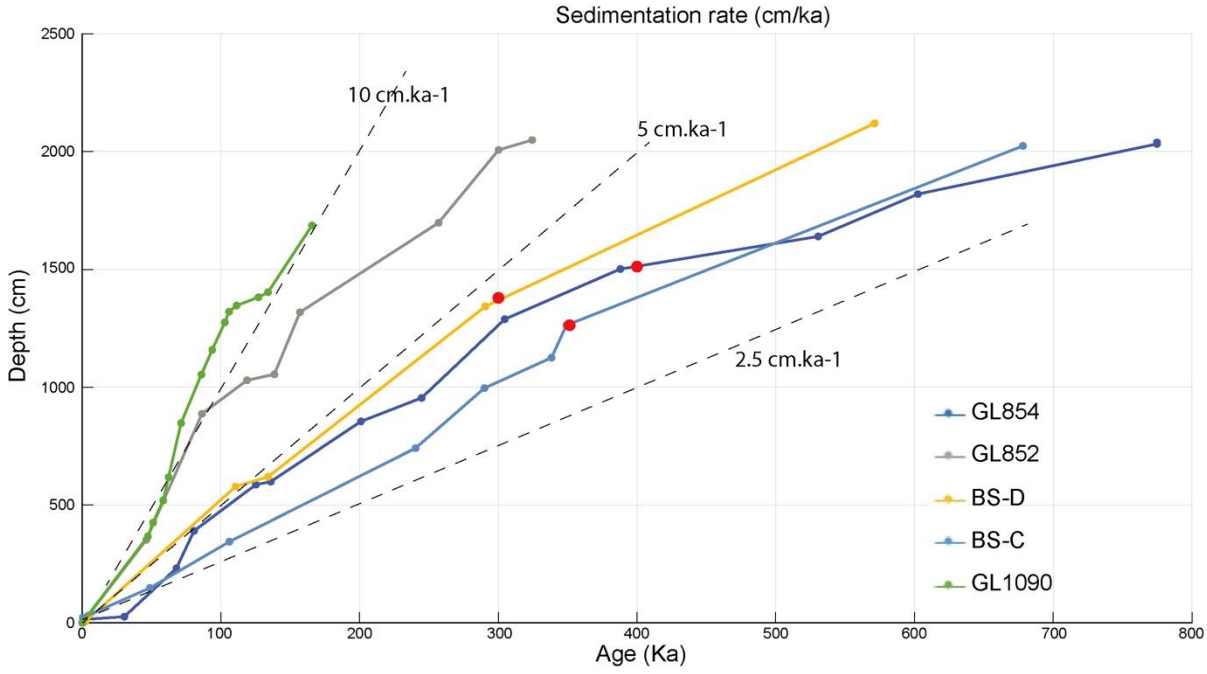

***Figure 10**: Sedimentation rates from published cores (see Table 1 for references). In dashed black lines constant sedimentation rates (2.5; 5; and 10 cm/ka).*

Finally, we also calculated sedimentation rates for each glacial and each interglacial (defined from the isotopic curves and the core description). Results are shown in Table 3. On average values are quite similar.

		GL852		**GL854**		**BS-C**		**BS-D**	
Top MIS	Ages (ka)	Thick-ness (cm)	Sed. Rate (cm/ka)	Thick-ness (cm)	Sed. Rate (cm/ka)	Thick-ness (cm)	Sed. Rate (cm/ka)	Thick-ness (cm)	Sed. Rate (cm/ka)
MIS 1	0-11.6	139.06	11.99	21.11	1.82	38.29	3.30	100.00	8.62
MIS2	11.6-24	176.56	14.24	14.82	1.19	53.19	4.29	77.78	6.27
MIS 3-4-5	24-130	909.36	8.58	558.57	5.27	414.88	3.91	562.24	5.30
MIS 6	130-190	450.00	7.50	220.03	3.67	423.39	7.06	324.45	5.41
MIS 7	190-244	260.94	4.83	163.27	3.02	206.38	3.82	288.90	5.35
MIS 8	244-301	215.63	3.78	283.78	4.98	161.70	2.84	173.33	3.04
MIS 9	301-334			127.03	3.85	248.93	7.54	264.45	8.01
MIS 10	334-364			114.12	3.80	297.87	9.93	157.78	5.26
MIS 11	364-427			57.50	0.91	85.11	1.35	171.11	2.72
MIS 12	427-474			68.63	1.46	206.38	4.39	126.67	2.70
MIS 13	474-528			43.53	0.81	165.95	3.07	157.78	2.92
MIS 14	528-568			87.83	2.20	80.85	2.02	131.12	3.28

MIS 15	568-712			120.99	0.84	148.93	1.03		
MIS 16	712-760			56.03	1.17				

Table 3*: Sedimentation rates calculated from the lithological log and the isotopic stages (Figures 8 and 9)*

5. Discussion

5.1. Significance of reflectors

The correlation of continuous reflectors in all the areas and their dating by cores in different zones show that they have a coherent, regional and even global consistency. The eight continuous reflectors on the slope (R1 to R8) correspond to the top of the MIS glacial maxima dated MIS2 to MIS18 by the cores. In other words, strong reflectors are related to the glacial/interglacial transition or terminations of each 100,000 years cycles. The reflectors, therefore, correspond to a Maximum Regressive Surface (MRS as defined in Catuneanu, 2019), which is also merged (at the scale of the chirp resolution) with the following transgressive surface related to the rapid deglaciation of each 100,000 years glacio-eustatic cycles. This is a common feature observed on many margins for Quaternary seismic sequences related to the asymmetric characteristic of late Quaternary glacio-eustatic cycles with long-trend cooling phase/sea-level drop (70-90 ka) and short transgression/sea-level rise (10 ka).

A nicely documented example is given by the Gulf of Lion, Mediterranean Sea, with good-quality, very high-resolution seismic data, and the detailed analysis of long cores in the PROMESS PRGL1-4 borehole by 300m water depth. In this case study, Rabineau et al. (2005) and Sierro et al. (2009) showed that the Maximum Regressive Surface on the upper slope was marked by a strong reflection that corresponded to the transition from terrigenous mud-silt sediment to a thin sandy-size layer with a concentration of foraminiferal tests accumulated during the transgressive phase just after the last glacial maximum (LGM). What is somehow surprising here is that the study area is well out of the direct influence of sea-level changes as all the areas are over 2000m of water depth.

Information from the cores show that glacial/interglacial cycles are characterized by differential lithologies, as shown in the result section and summarized on the synthetic lithological log (Figure 11). More specifically, the glacial/interglacial terminations are always characterized by a change from low clay/silt ratio with occasional thin sand layers during the glacial and a

marl layer (just above) with a high content in carbonate which characterizes the transgression, which is clearly seen as a peak in the %CaCO3 curve of core GL-854 for example (Figure 8) but also identified in the lithological logs of all cores (Figures 8 and 9). The recent study from Mathias et al. (2021) centered on GL-1090 provided also lithological data with a description of "mixed silt and clay with minor contribution of sand (<1%) detected only in four samples". Unfortunately, we do not know where those four samples were taken. But Mathias et al. (2021) also add that they "observed a decrease in the clay/silt ratio, i.e. with a decrease in the proportion in the finest particle, reaching a minimum around the last two terminations TII and I1, and a maximum ratio during MIS5e (more clays). On the other hand, the early interglacial (just after the glacial) are made by whitish clays with a large amount of carbonates (marl facies with 30-60 % carbonates).

All these observations tend to show that there is, indeed, a change in lithologies at the glacial/interglacial terminations that creates an impedance contrast that is shown in our very high-resolution chirp profiles by the high amplitude reflectors Ri.
The rest of the sequence/cycle is characterized by clay-dominated mud with variable percentage of carbonates, which corresponds to a transparent layer on the chirp profiles.

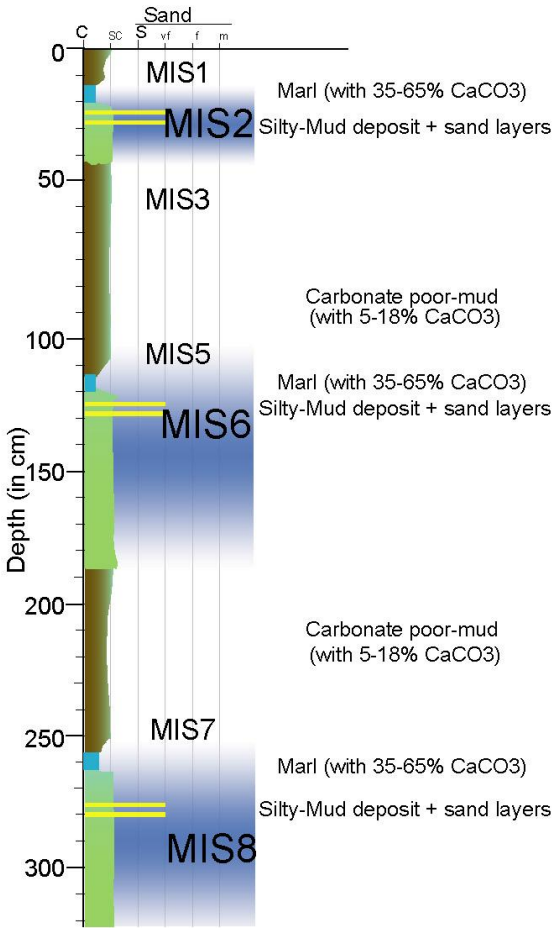

Figure 11 *Synthetic characteristics of lithologies from the cores, with Silty-mud and sand layers during Glacial Maxima and marl (35-65% CaCO3) deposited at transitions between glacial/interglacial followed by carbonate-poor mud.*

The record of smaller-scale sea-level drop and flooding events can also be registered locally in the form of a reflector (but with smaller amplitudes than the Glacial Maxima-Termination of 100,000 years cycles). However, these events (and related reflectors) in the slope of Santos Basin are recorded only in areas with higher sedimentation rates, such as in depression (mini basins), as shown on Figure 3 for example. Similar record of high-resolution sea-level drop and flooding events as visible seismic reflectors was also demonstrated elsewhere. In the case of the Gulf of Lion (NW Mediterranean Sea) for MIS3, for example (Jouet et al., 2006). In the Santos Basin case, because of smaller sedimentation rates, such events are not always visible, but main stadials, such as MIS4, MIS7b, and MIS 9b have been recorded in the area when sedimentation rates reach around 10 $cm.ka^{-1}$, such as through core GL1090 and GL 852 (Figures 3, 4, 5 and 8).

5.2. Origin of sediment: sources and processes

Results from seismic and cores show that glacial/interglacial cycles record a variable amount of terrigenous material along the 100,000 years cycles together with a variable percentage of Carbonates. For the terrigenous detrital particles of silt and sand, we might seek for an increased role of the small rivers coming from the Serra do Mar during glacial intervals, together with an increased erosion of the shelf in subaerial position during glacial maxima. For the carbonates, in the southwestern Atlantic, the study of planktonic foraminiferal records has suggested that productivity was higher during deglaciation than in the LGM and the Holocene (Toledo et al., 2007b). This is also recorded in the lithologies with the highest percentage of carbonates during the transgression/deglaciation (Figure 11). This highest productivity during deglaciation is also attested by Reis et al. (2013), who showed that carbonate build-ups were formed on the outer shelf of the Northern Santos Basin during transgressions, and that they were then eroded during subsequent regressions.

Previous studies on the outer shelf and upper slope of the study area also documented a change in lithology from LGM to present-day, with enrichment in calcium carbonate and organic carbon towards the recent (de Mahiques et al., 2002). The authors suggested that during the LGM the shelf waters were more influenced by the Coastal Water, with a narrower shelf surface and a more effective input of terrigenous material to the continental slope during LGM. This oceanward shift of input has been also described for the Amazon River outflow plume during cold climates (Wilson et al., 2011). However; considering the water depth of cores and seismic data into consideration (around 2,000 m) and the modest size of coastal rivers, we also have to consider an indirect input brought by currents. Most studies describe the prevalence of very fine sands and silty sands resulting from submarine processes, both gravitational (across slope) and contouritic (along slope), together with pelagic muddy sedimentation (e.g., Duarte and Viana, 2007; de Mahiques et al., 2021b).

The recent study of Mathias et al., (2021) that studied in detail one core used in this paper (GL-1090) with multiple proxies, states that the terrigenous sediments at this core location GL1090 derived from the Plata River (southeastern South America). This material was transported northwards by the Brazilian Coastal Current (BCC, Figure 1), and their delivery to our core site was modulated by sea-level oscillations. Periods of low sea-level were characterized by the input of coarser and more abundant terrigenous sediments. Other authors also suggested the key role of the Plata River as the source of sediments in the Santos Basin (Souza and Robinson, 2004; Nagai et al., 2014; de Mahiques et al., 2020).

A complete provenance study could not be undertaken on the cores discussed in this study. However, by combining observation from lithologies and earlier studies, we suggest that sediments on the slope of the Santos Basin are a combined mix of (1) fine sediments originating from the Plata River and transported northward by the Brazilian Coastal Current, that is more efficient and shifted eastward by the shorter width of the shelf at glacial maxima (2) direct input from the coastal rivers running from the Serra do Mar with increased incision due to their lowered base-level and (3) in-situ cannibalization of shelf sediments deposited during highstand phase of the G/IG cycle. We suggest that this last source of sediment is responsible for the formation of the thin sand layers observed (and inferred) in the cores that probably correspond to turbidites originating from the shelf edge.

5.3. Why a major change after MIS12 (Termination V)?

A major change at MIS12 is shown by a consistently strong change in sedimentation rates, as shown in the available cores for this study: sedimentation rates are relatively constant from the base of the cores to MIS12. Then, they show a strong increase in sedimentation rates from MIS12-MIS11 to the present day (Figure 10). This is also seen throughout the spacing of reflectors on the sub-bottom profiles, as well as in the sedimentation rates, which are stronger for the cores spanning only the last cycles (Table 2).

This change in sedimentation rates is also very well seen in a core CDH-79 from the equatorial Brazilian margin (Para-Maranhão Basin), just south of the Amazon River (Ferreira et al., 2021); this study shows an age-model with a sudden change in sedimentation rates around 400 ka, although this change is not really commented in their text. Our measurements from their study show an average rate of 1.33 cm/ka from 2 Ma to 400 ka (at 1200cm core -depth) and a jump to an average rate around 3 cm/ka after 400 ka (e.g., after MIS12) (with an additional hiatus described by the authors at 50-60cm around 30 ka). Therefore, the change occurring at around MIS12 (400 ka) seems to have a regional record in the South Atlantic. It might be explained by a late installation of the MPT and/or an increase in currents bringing sediments to the zone.

However, this change also corresponds to the Mid-Brunhes event (MBE) centered around 400 ka and described worldwide (e.g., Jansen et al., 1986; Nagender et al., 2013; Yin and Berger, 2010; Barth et al., 2018; Park et al., 2022). The MBE is characterized by a global increase in carbonate production, linked to nutrient flux and upwelling increased intensity (Flores et al., 2012). The Mid-Brunhes Event ~400,000 years ago also corresponds to enhanced Arctic am-

plification (Cronin et al., 2017). In the Gulf of Lion, the sea level dropped to a depth of -102 +/- 6m during the last three glaciations (MIS2, MIS6, MIS8) but reached exceptionally low values of more than -150 +/- 10m during the preceding glaciations MIS10 and MIS 12 at about 340 and 434 kyr BP (Rabineau et al., 2006).

Droxler and Jorry, 2013 described MIS 11 as a "Superinterglacial" at + 6m above present-day sea-level and with a duration of 30 ka (i.e., longer than other interglacials whose mean duration is around 10 ka; e.g., Philander, 2008) and that corresponds to the start of true tropical reef, neritic carbonates build-ups: "This exceptionally high-amplitude (>120-m) sea-level transgression—the first such transgression since the onset of the main Northern Hemisphere glaciations 2.7–2.5 Mya—and the unusually long-lasting MIS 11 (Raynaud et al., 2003) dramatically contrast with the overall early-middle-Pleistocene lowering of the marine base level, which was tied to the establishment and expansion of the major continental ice sheets in the Northern Hemisphere" (Droxler and Jorry, 2013).

In our study area, this MIS11 is also an outstanding interglacial as it is the only one that develops a layer of Nanno Foram Ooze, clearly identified on cores BS-C and BS-D.
All the observations made worldwide at the MBE explain the specificity of this layer deposited during MIS11 and the increase in sedimentation rates that we observe. However, we think that it cannot, alone, explain the doubling of the rates, and we also infer an increase in terrestrial (probably indirect) input.

The abrupt change occurring at 400 ka might also be the imprint of larger-scale 400 ka Milankovitch cycles as proposed in Rabineau et al., 2006 for the change in sea-level amplitudes observed in the Gulf of Lion at the same time. Further studies and longer cores would be needed to test this hypothesis.

5. Conclusion

This study shows that the upper slope of the Santos Basin exhibits a nice preservation of the last ~800,000 years with the record of every 100,000 years climatic cycles. The prominent reflectors on the very high-resolution chirp profiles appear at the glacial/interglacial transitions with a change in lithologies with more terrigenous sediments during glacials and more carbonates-rich marl during deglaciation. We see the importance of interpreting existing chirp

profiles that clearly enable the recognition of climate cycles on the South-Eastern Brazilian margin. A doubling of sedimentation rates is also observed after the MIS12-11 transition around 400 ka, which seems to be related to a change in carbonate production and might also be related to 400 ka Milankovitch cycles. Therefore, the study brings new interpreted vertical images of sediment deposition and architecture of the South-eastern Brazilian margin at high resolution in a chronostratigraphic framework and in relation to global Quaternary climatic cycles.

Acknowledgements

This study is part of the SANBA project (**San**tos **Ba**sin experiment), conducted by IFREMER (France) and Petrobras (Brazil), in collaboration with the CNRS (France), the Universidade de Brasilia (Brazil), the Faculdade de Ciências da Universiade de Liboa (Portugal) and the Université de Bretagne Occidentale (France). We would like to thank the captain, crew and MCS technical team of the R/V L'Atalante during the SANBA cruise operated by the "Flotte océanographique française" (Aslanian et al., 2010a and 2010b). Any request has to be addressed to Daniel Aslanian (aslanian@ifremer.fr) and Adriano Viana (avaina@petrobras.com.br). Many thanks also to the OBS (J. Crozon, P. Pelleau, M. Roudaut, P. Fernagu, D. Le Piver, R. Apprioual), and land-station (M. Paula Ribas, J-L. Duarte) and Multi-channel Seismic technical teams who made this experiment possible and enabled acquisition of bathymetric and sub-bottom profiles used in this study. Thanks are due to Lucas Tortarolo who prepared Figure 1-D. Authors would like to acknowledge editors and reviewers for their useful comments that greatly improved our manuscript.

CRediT authorship contribution statement

The SANBA Project was led and funded by D. Aslanian and M. Moulin, from Ifremer, and A. Viana, from Petrobras.

Marina Rabineau: Writing – _original draft, Methodology, Investigation, Formal analysis, Data curation, Conceptualization, Writing – _review & editing. **Massinissa Benabdellouahed**: Investigation, Formal analysis, Data curation, Writing – _original draft. **Agnes Baltzer**: Writing – _original draft, Methodology, Investigation, Formal analysis, Data curation. **Romain Pellen:** Data curation, Writing – _review & editing. **AntonioTadeu dos Reis**: Methodology, Investigation, Formal analysis, Data curation, Writing – _review & editing. **Renata Maia**: Methodology, Investigation, Formal analysis, Data curation, Writing – _review & editing. **Zohra Mokeddem**: Methodology, Investigation, Formal analysis, Data curation. **Sidonie Révillon:** Methodology, Investigation, Formal analysis. **Philippe Schnurle**: Investigation, Formal analysis, Data curation. **Karen Costa**: Methodology, Investigation, Formal analysis, Data curation, Writing – _review & editing. **Felipe Toledo**: Methodology, Investigation, Formal analysis, Data curation, Writing – _review & editing. **Estelle Leroux**: Data curation, Writing – _review & editing. **Maryline Moulin**: Methodology, Investigation, Data curation, Conceptualization, Writing – _review & editing, Funding acquisition **A. Roessler Viana**: Methodology, Investigation, Data curation, Conceptualization, Writing – _review & editing, Funding acquisition. **D. Aslanian**: Methodology, Investigation, Data curation, Conceptualization, Writing – _review & editing, Funding acquisition.

Funding: This research was funded by Petrobras (Brazil) and Ifremer (France). The data set collected during the SANBA experiment are protected under a partnership with Petrobras. Any request has to be addressed to Daniel Aslanian (aslanian@ifremer.fr) and Adriano Viana (aviana@petrobras. com.br). Some SANBA cruise raw dataset (bathymetry and chirp profiles) are available at https://doi.org/10.17600/10010150 and https://doi.org/10.17600/10010160

The authors would like to thank for their additional financial support CAPES-COFECUB and CNRS. This work was also supported by Labex Mer and ISblue project, Interdisciplinary graduate school for the blue planet (ANR-17-EURE-0015) and co-funded by a grant from the French government under the program "Investissements d'Avenir" embedded in France (2030). Antonio Tadeu dos Reis received research grant No. 309779/2021-9 from the Brazilian National Research Council (CNPq). Massinina Benabdellouahed received a grant from Region Bretagne.

Declaration of competing interest The authors declare that they have no known competing financial interests or personal relationships that could have appeared to influence the work reported in this paper.

REFERENCES :

Almeida, F.K., de Mello, R.M., Costa, K.B., Toledo, F.A.L. 2015. The response of deepwater benthic foraminiferal assemblages to changes in paleoproductivity during the Pleistocene (last 769.2 kyr), western South Atlantic Ocean. Palaeogeogr. Palaeoclimatol. Palaeoecol. 440, 201–212.

Artusi, L., Jr, F., De, A.G. 2007. Sismografia rasa da plataforma continental de Cabo Frio - Araruama - RJ. *Rev. Bras. Geofísica* 25, 7–16. doi:10.1590/S0102-261X2007000500002

Aslanian, D., Moulin, M., Olivet, J. L., Unternehr, P., Matias, L., Bache, F., Rabineau, M., Nouzé, H., Klingelhoefer, F., Contrucci, I. and Labails, C. 2009. Brazilian and African passive margins of the Central Segment of the South Atlantic Ocean: Kinematic constraints. Tectonophysics, 468(1-4), 98-112.

[dataset] Aslanian, D., Klingelhoeffer, F., Moulin, M. 2010a. SANBA cruise, LEG1, RV L'Atalante, https://doi.org/10.17600/10010150

[dataset] Aslanian, D., Klingelhoeffer, F., Moulin, M. 2010b. SANBA cruise, LEG2, RV L'Atalante, https://doi.org/10.17600/10010160

Barth, A. M., Clark, P. U., Bill, N. S., He, F., and Pisias, N. G. 2018. Climate evolution across the Mid-Brunhes transition. *Climate of the Past, 14*(12), 2071-2087.

Bassetti, M.A., Berne, S., Jouet, G., Taviani, M., Dennielou, B., Flores, J.A., Gaillot, A., Gelfort, R., Lafuerza, S., Sultan, N. 2008. The 100-ka and rapid sea level changes recorded by prograding shelf sand bodies in the Gulf of Lions (western Mediterranean Sea). *Geochem. Geophys. Geosystems*, doi:10.1029/2007GC001854

Bassinot, F.C., Labeyrie, L.D., Vincent,E., Quidelleur,X., Shackleton,N.J., Lancelot,Y. 1994. The astronomical theory of climate and the age of the Brunhes Matuyama magnetic reversal. *Earth and Planetary Science Letters*, **126(1-3)**, 91-108

Berger, W.H., Wefer, G. 1996. Expeditions into the Past: Paleoceanographic Studies in the South Atlantic, in: The South Atlantic. Springer Berlin Heidelberg, pp. 363–410.

Berne, S., Jouet, G., Bassetti, M.-A., Dennielou, B., Taviani, M. 2007. Late Glacial to Preboreal sea-level rise recorded by the Rhône deltaic system (NW Mediterranean). Mar. Geol. 245, 65–88.

Bueno, G.V., Machado, Jr, D. L., de Oliveira, J. A. B. And Marques, E., J., J. 2004. A Influência do "Lineamento Capricórnio" na Evolução Tectono-Sedimentar da Bacia de Santos, *in* Congresso Brasileiro de Geologia, 52, Araxá. Anais, Sociedade Brasileira de Geologia, Simpósio 28 – Petróleo: geologia e exploração, T 773.

Cainelli, C., Mohriak, W.U. 1999. Some remarks on the evolution of sedimentary basins along the Eastern Brazilian continental margin. Episodes-Newsmag. Int. Union Geol. Sci. 22, 206–216.

Camillo, E., Quadros, J. P., Santarosa, A. C. A., Costa, K. B., Toledo, F. A.L.2020. An Abrupt Cooling Event Recorded Around 73 Kyr In Western South Atlantic. Quaternary International, v. 542, p. 80-87.

Carminatti, M., Scarton, J.C. 1991. Sequence Stratigraphy of the Oligocene Turbidite Complex of the Campos Basin, Offshore Brazil: An Overview, in: Weimer, P., Link, M.H. (Eds.), Seismic Facies and Sedimentary Processes of Submarine Fans and Turbidite Systems, Frontiers in Sedimentary Geology. Springer New York, pp. 241–246.

Catuneanu O. 2019. Model-independent stratigraphy, Earth-Science Reviews, 188, p. 312-388. doi.org/10.1016/j.earscirev.2018.09.017

Chang, H.K., Kowsmann, R.O., Figueiredo, A.M.F., Bender, A. 1992. Tectonics and stratigraphy of the East Brazil Rift system: an overview. Tectonophysics, Geodynamics of Rifting, Volume II Case History Studies on Rifts: North and South America and Africa 213, 97–138. doi:10.1016/0040-1951(92)90253-3

Chiessi, C., Mulitza, S., JeroenGroeneveld, J., Silva, J.B., Campos, M.C., Gurgel, M.H.C. 2014. Variability of the Brazil Current during the late Holocene, Palaeogeography, Palaeoclimatology, Palaeoecology, Volume 415, Pages 28-36, https://doi.org/10.1016/j.palaeo.2013.12.005.

Cogné, N., Gallagher, K., Cobbold, P.R. 2011. Post-rift reactivation of the onshore margin of southeast Brazil: Evidence from apatite (U–Th)/He and fission-track data. Earth Planet. Sci. Lett. 309, 118–130. doi:10.1016/j.epsl.2011.06.025

Cogné, N., Gallagher, K., Cobbold, P.R., Riccomini, C., Gautheron, C. 2012. Post-breakup tectonics in southeast Brazil from thermochronological data and combined inverse-forward thermal history modeling. J. Geophys. Res. Solid Earth 117, B11413. doi:10.1029/2012JB009340

Contreras, J., Zühlke, R., Bowman, S., Bechstädt, T. 2010. Seismic stratigraphy and subsidence analysis of the southern Brazilian margin (Campos, Santos and Pelotas basins). Mar. Pet. Geol. 27, 1952–1980. doi:10.1016/j.marpetgeo.2010.06.007

Costa, K. B., Camillo Jr, E., Santarosa, A. C. A., Iwai, F. Sayuri, Quadros, J. P., Leipnitz, I. I., Toledo, F. A. L. 2018. Menardiiform planktonic foraminifera stratigraphy from Middle Pleistocene to Holocene in the Western South Atlantic. Revista Brasileira De Paleontologia, v. 21, p. 225-237.

Cronin, T. M., Dwyer, G. S., Caverly, E. K., Farmer, J., DeNinno, L. H., Rodriguez-Lazaro, J., Gemery, L. 2017. Enhanced Arctic amplification began at the Mid-Brunhes Event~ 400,000 years ago. *Scientific Reports*, *7*(1), 1-7.

de Mahiques M.M., Silveira I.C.A., Sousa S.H.M., Rodrigues M. 2002. Post-LGM sedimentation on the outer shelf–upper slope of the northernmost part of the São Paulo Bight, southeastern Brazil. Mar Geol 181: 387–400. doi:10.1016/S0025-3227(01)00225-0

de Mahiques M.M., Tessler M.G., Ciotti A.M., Silveira I.C.A., Sousa S.H.M., Figueira R.C.L., Tassinari C.C.G., Furtado V.V., Passos R.F. 2004. Hydrodynamically driven patterns of recent sedimentation in the shelf and upper slope off Southeast Brazil. Cont Shelf Res 24: 1685–1697. doi:10.1016/j.csr.2004.05.013

de Mahiques, M. M., Figueira, R. C. L. , Sousa, S. H. M. , Santos,R. F, Ferreira, P. A. L., Kim, B.S.M Cazzoli y Goya, S.,Matos,M.C.S.N, Bicego, M.C. 2020. Sedimentation on the southern Brazilian shelf mud depocenters: Insights on potential source areas,Journal of South American Earth Sciences, Volume 100,https://doi.org/10.1016/j.jsames.2020.102577

de Mahiques, M.M. ; Violante, R., Franco-Fraguas, P., Burone, L., Rocha, C. B. Ortega, L., dos Santos, R.F., Mi Kim, B.S. ; Figueira, R. C.L. and Bícego, M. C. 2021a. Control of oceanic circulation on sediment distribution in the southwestern Atlantic margin (23 to 55°S). Ocean Sci., 17, 1213-1229. https://doi.org/10.5194/os-17-1213-2021

de Mahiques, M.M., Cazzoli Y Goya, S., de Matos, M.C.S.N,, Udenal de Oliveira, R.A., Mi Kim, B.S., Ferreira, P.A.F., Figueira, R. C.L., Bícego, M. C. 2021b. Grain-Size End-Members And Environmentally Sensitive Grain-Size Components: A Comparative Study In The Mud Shelf Depocenters Off Southern Brazil. International Journal Of Sediment Research, v. 36, p.

de Menocal, P.B. 2004. African climate change and faunal evolution during the Pliocene-Pleistocene. Earth and Planetary Science Letters (Frontiers). 220, 1/2, 3-24. 2004.

dos Santos Filho, J.R., A.G. Figueiredo, J.C. Carneiro, et al., 2022. Mesophotic bioclastics and bioconstructions at the continental shelf of Santos Basin, Brazil, Sedimentary Geology. https://doi.org/10.1016/j.sedgeo.2022.106294

Droxler, A.W., Alley, R.B., Howard, W.R., Poore, R.Z., Burkle, L.H. 2003. Unique and Exceptionally Long Interglacial Marine Isotope Stage 11: Window Into Earth Warm Future Climate. AGU Geophysical Monograph Series, Book Editor(s): André W. Droxler, Richard Z. Poore, Lloyd H. Burckle, https://doi.org/10.1029/137GM01

Droxler, A.W. and Jorry, S.J. 2013. Deglacial Origin of Barrier Reefs Along Low-Latitude Mixed Siliciclastic and Carbonate Continental Shelf-Edges. Annual Review of Marine Science, Vol 5, 5, 165-190.

Duarte, S. L. and Viana, A. R., 2007. Santos Drift System: stratigraphic organization and implications for late Cenozoic palaeocirculation in the Santos Basin, SW Atlantic Ocean. Geological Society, London, Special Publications, 276, 171-198, 1 January 2007, https://doi.org/10.1144/GSL.SP.2007.276.01.09

Evain, M., Afilhado, A., Rigoti, C., Loureiro, A., Alves, D., Klingelhoefer, F., Schnurle, P., Feld, A., Fuck, R., Soares, J., de Lima, M. v., Corela, C., Matias, L., Benabdellouahed, M., Baltzer, A., Rabineau, M., Viana, A., Moulin, M., Aslanian, D. 2015. Deep structure of the Santos Basin-Sa˜o Paulo Plateau System, SE Brazil. J. Geophys. Res. Solid Earth 120, 5401–5431. doi:10.1002/2014JB011561

Evans, M.E. Heller, F. 2003. Environmental Magnetism – Principles and Applications of Enviromagnetics (first ed), Academic Press, San Diego

Faugères, J.C., Imbert, P., Mézerais, M.L., Cremer, M. 1998. Seismic patterns of a muddy contourite fan (Vema Channel, South Brazilian Basin) and a sandy distal turbidite deep-sea fan (Cap Ferret system, Bay of Biscay): a comparison. Sediment. Geol. 115, 81–110.

Ferreira, F., Leipnitz, I. I., Vicalvi, M. A., Sanjinés, A., Enrique S. 2012. Zoneamento Paleoclimático Do Quaternário Da Bacia De Santos Com Base Em Foraminíferos Planctônicos. Revista Brasileira De Paleontologia, v. 15, p. 173-188.

Ferreira, P.A., de L., Costa, K.B., Toledo, F.A. de L., Figueira, R.C.L. 2015. Sedimentation rates and age modeling of Late Quaternary marine sediments with unsupported 230Th. J. Radioanal. Nucl. Chem. 304, 829–836. doi:10.1007/s10967-014-3905-4

Ferreira, P. A., de Lima, R. C. L. F., Cazzoli y Goya, S., de Mahiques, M.M. "Insights on the marine sedimentation of the continental shelf and upper slope off SE Brazil during the 20th century with natural radionuclides" *Regional studies in marine science* 39, (2020): 101466. doi: 10.1016/j.rsma.2020.101466.

Ferreira, F., Silva, C. G., Oliveira, A. S., Chiessi, C.M., Kern, A. K., Baker, P. A., Dwyer, G., Rigsby, C. A., Huang, E., Tian, J. 2021 . Biochronostratigraphy Of The Western Equatorial Atlantic For The Last 1.93 Ma. Quaternary International, v. 598, p. 24-37. http://dx.doi.org/10.1016/j.quaint.2021.04.042

Fleming, F.P., Maia, R.M.C., Reis, A.T., Alves, E.C., Gorini, C., Silva, C.G., Guerra, J.V. 2009. Variability and Evolution of Shallow Continental Shelf Systems off Rio de Janeiro State, Santos Basin—Brazil. J. Coast. Res. 617–621.

Friederichs, Y.L., Reis, A.T., Silva, C.G., Toulemonde, B., Maia, R.M.C., Guerra, J.V. 2013. The seismic architecture of the Sepetiba fluvio-estuarine system preserved on

the shallow stratigraphic record on the offshore inner-mid shelf, Rio de Janeiro, Brazil. Brazilian Journal of Geology 43, 124–138 (in Portuguese).

Flores, J.A., Filippelli, G.M., Sierro, F.J., Latimer, J. 2012. The "White Ocean" hypothesis: a late Pleistocene Southern Ocean governed by coccolithophores and driven by phosphorus. Front. Microbiol. 3, 233. http://dx.doi.org/10.3389/fmicb.2012.00233.

Garcia, S.F. de M., Letouzey, J., Rudkiewicz, J.-L., Danderfer Filho, A., Frizon de Lamotte, D. 2012. Structural modeling based on sequential restoration of gravitational salt deformation in the Santos Basin (Brazil). Mar. Pet. Geol. 35, 337–353. doi:10.1016/j.marpetgeo.2012.02.009

Garfield, N. 1990. The Brazil Current at subtropical latitudes. PhD Thesis Univ. R. I. 122.

Gibbard, P.L., Head, M.J. 2009. The definition of the Quaternary system/era and the Pleistocene series/epoch. Quat. Rev. Assoc. Fr. Pour Létude Quat. 20, 125–133.

Gonçales De Souza, K. 1991. La marge continentale brésilienne sud-orientale et les domaines océaniques adjacents: structure et evolution.

Grant, K., Rohling, E., Ramsey, C. et al. 2014. Sea-level variability over five glacial cycles. *Nat Commun* **5,** 5076. https://doi.org/10.1038/ncomms6076

Haug G.H., Ganopolski A., Sigman D.M., Rosell-Mele A., Swann G.E., Tiedemann R., Jaccard S.L., Bollmann J., Maslin M.A., Leng M.J., Eglinton G. 2005, North Pacific seasonality and the glaciation of North America 2.7 million years ago, *Nature*, 433, 821– 825, doi:10.1038/nature03332.

Head, M.J., Gibbard, P.L. 2015. Early–Middle Pleistocene transitions: Linking terrestrial and marine realms. Quat. Int., The Jaramillo Subchron and the Early-Middle Pleistocene transition in continental records from a multidisciplinary perspective 389, 7–46. doi:10.1016/j.quaint.2015.09.042

Head, M.J., Gibbard, P.L., van Kolfschoten, T. 2015. The Quaternary System and its formal subdivision. Quat. Int., The Quaternary System and its formal subdivision 383, 1–3. doi:10.1016/j.quaint.2015.06.038

Hogg, N., Biscaye, P., Gardner, W., Schmitz Jr, W.J. 1982. On the transport and modification of Antarctic Bottom Water in the Vema Channel. J Mar Res 40, 231–263.

Holden, P.B., Edwards, N.R., Wolff, E.W., Valdes, P.J. and Singarayer, J.S. (2011), The Mid-Brunhes Event and West Antarctic ice sheet stability. J. Quaternary Sci., 26: 474-477. https://doi.org/10.1002/jqs.1525

Howard, W.R. 1997. Palaeoclimatology: A warm future in the past. Nature 388, 418–419. doi:10.1038/41201

Jansen, J.H.F., Kuijpers, A., Troelstra, S.R. 1986. A Mid-Brunhes climatic event: long-term changes in global atmosphere and ocean circulation. Science 232 (4750), 619–622

Jouet, G., Berné, S., Rabineau, M., Bassetti, M.A., Bernier, P., Dennielou, B., Sierro, F.J., Flores, J.A., Taviani, M. 2006. Shoreface migrations at the shelf edge and sea-level changes around the Last Glacial Maximum (Gulf of Lions, NW Mediterranean). Mar. Geol., EUROSTRATAFORM VOL. 1: Source to Sink Sedimentation on the European Margin 234, 21–42. doi:10.1016/j.margeo.2006.09.012

Kim, S., Yoo, K-C., Lee, J.Il., Lee M. K., Kim, K., Yoon, H.Il., Moon H. S. (2018). Relationship between magnetic susceptibility and sediment grain size since the last glacial period in the Southern Ocean off the northern Antarctic Peninsula – Linkages between the cryosphere and atmospheric circulation, Palaeogeography, Palaeoclimatology, Palaeoecology,Volume 505, Pages 359-370, https://doi.org/10.1016/j.palaeo.2018.06.016.

Klingelhoefer,F., Evain, M., Afilhado, A., Rigoti, C., Loureiro, A., Alves, D., Leprêtre, A., Moulin, M., Schnurle, P., Benabdellouahed, M., Baltzer, A., Rabineau, M., Feld, A., Viana, A., Aslanian, D. (2015). Imaging proto-oceanic crust off the Brazilian Conti-

nental Margin. Geophysical Journal International, Volume 200, Issue 1, January 2015, Pages 471–488.

Kolla, V., Biondi, P., Long, B., Fillon, R. 2000. Sequence stratigraphy and architecture of the late Pleistocene Lagniappe delta complex, northeast Gulf of Mexico. Geol. Soc. Spec. Publ. 172, 291–327.

Lafosse M., Gorini C., Le Roy P., d'Acremont E., Alonso B., Ercilla G., Rabineau, M., Vázquez J.T., Rabaute, A., Ammar A. 2018. Late Quaternary-Holocene history of a tectonically active Morocco continental margin (Nekor Basin, Western Mediterranean, Morocco), Marine and Petroleum Geology, 97, p. 370-389

Lambeck, K., Yokoyama, Y., Purcell, T. 2002. Into and out of the Last Glacial Maximum: sea-level change during Oxygen Isotope Stages 3 and 2. Quat. Sci. Rev., EPILOG 21, 343–360. doi:10.1016/S0277-3791(01)00071-3

Le Roy, P., Sahabi, M., Maad, N., Rabineau, M., Gutscher, M.-A., Babonneau, N., Van Vliet Lanoe, B., Ait Brahim, L., M'hammdi, N., Trentesaux, A., Dakki, M., Hssain, M. 2014. 3D architecture of Quaternary sediment along the NW Atlantic Moroccan Rharb continental shelf: A stratal pattern under the dual control of tectonics and climatic variations. Mar. Pet. Geol. 49, 129–142. doi:10.1016/j.marpetgeo.2013.10.003

Lessa, D. V.O., Santos, T. P., Venancio, I. M., Albuquerque, A. L. S. 2017. Offshore Expansion Of The Brazilian Coastal Upwelling Zones During Marine Isotope Stage 5. Global And Planetary Change, v. 158, p. 13-20.

Lima, A.F., Faugeres, J.-C., Mahiques, M., 2009. The Oligocene-Neogene deep-sea Columbia Channel system in the South Brazilian Basin; seismic stratigraphy and environmental changes. Mar. Geol. 266, 18–41. doi:10.1016/j.margeo.2009.07.009

Lisiecki, L.E., Raymo, M.E. 2005. A Pliocene-Pleistocene stack of 57 globally distributed benthic δ18O records. Paleoceanography 20, PA1003. doi:10.1029/2004PA001071

Lisiecki, L.E., Raymo, M.E. 2007. Plio-Pleistocene climate evolution: trends and transitions in glacial cycle dynamics, Quaternary Science Reviews, 26, Issues 1-2, p. 56-69. doi:10.1016/j.quascirev.2006.09.005

Liu, J.P., Milliman, J.D., Gao, S., Cheng, P. 2004. Holocene development of the Yellow River's subaqueous delta, North Yellow Sea. Mar. Geol. 209, 45–67. doi:10.1016/j.margeo.2004.06.009

Lourenço, R. A., Mahiques, M. M., Wainer, I., Rosell Melé, A., Bicego, M. C. 2016. Organic biomarker records spanning the last 34,800 years from the southeastern Brazilian upper slope: links between sea surface temperature, displacement of the Brazil Current, and marine productivity. Geo Marine Letters, v. 36, p. 361-369.

Lowrie, A. 1986. Model for Fine-Scale Movements Associated with Climate and Sea Level Changes along Louisiana Shelfbreak Growth Faults 36.

Maia, R.M. da C., Reis, A.T. dos, Alves, E. da C., Silva, C.G., Guerra, J.V., Gorini, C., Silva, A., Arantes-Oliveira, R. 2010. Architecture and stratigraphic framework of shelf sedimentary systems off Rio de Janeiro state, Northern Santos Basin-Brazil. Braz. J. Oceanogr. 58, 15–29. doi:10.1590/S1679-87592010000500003

Marino, M., Maiorano, P., Lirer, F., Pelosi, N. 2009. Response of calcareous nannofossil assemblages to paleoenvironmental changes through the mid-Pleistocene revolution at Site 1090 (Southern Ocean). Palaeogeogr. Palaeoclimatol. Palaeoecol. 280, 333–349. doi:10.1016/j.palaeo.2009.06.019.

Marsset, B., Thomas, Y., Sultan, N., Gaillot, A. Stephan, Y. 2012. A multi-disciplinary approach to marine shallow geohazard assessment. Near Surface Geophysics, Volume 10, Issue 4, May 2012, p. 279 - 288

Martínez-Dios, A., Carles Pelejero, Sara Cobacho, Juancho Movilla, Jaume Dinarès-Turell, Eva Calvo, 2021. A 1-Million-Year Record of Environmental Change in the Central

Mediterranean Sea From Organic Molecular Proxies. Paleoceanography and Paleoclimatology, vol. 36, Issue 10. https://doi.org/10.1029/2021PA004289

Maslin, M.A., Ridgwell, A.J. 2005. Mid-Pleistocene revolution and the "eccentricity myth." Geol. Soc. Lond. Spec. Publ. 247, 19–34. doi:10.1144/GSL.SP.2005.247.01.02

Mathias, G. L., Roud, S. C., Chiessi, C. M., Campos, M. C., Dias, B. B., Santos, T. P., et al. 2021. A multi-proxy approach to unravel late Pleistocene sediment flux and bottom water conditions in the western South Atlantic Ocean. Paleoceanography and Paleoclimatology, 36, e2020PA004058.

Miller, K. G. et al. 2020. Cenozoic sea-level and cryospheric evolution from deep-sea geochemical and continental margin records.*Sci. Adv.***6**, eaaz1346(2020).DOI:10.1126/sciadv.aaz1346

Milliman, J.D. 1978. Morphology and structure of upper continental margin off southern Brazil. AAPG Bull. 62, 1029–1048.

Miranda, L.B. de, Castro, B.M. de, Kjerfve, B. 1998. Circulation and mixing due to tidal forcing in the Bertioga Channel, São Paulo, Brazil. Estuaries 21, 204–214. doi:10.2307/1352469

Mitchum, R.M., Vail, P. 1977. Seismic stratigraphic interpretation procedure. In: Payton, C.E. (Ed.), Seismic Stratigraphy – Applications to Hydrocarbon Exploration. In: AAPG Mem., pp. 135–143.

Modica, C.J., Brush, E.R. 2004. Postrift sequence stratigraphy, paleogeography, and fill history of the deep-water Santos Basin, offshore southeast Brazil. AAPG Bull. 88, 923–945.

Möller, O.O., Piola, A.R., Freitas, A.C., Campos, E.J.D., 2008. The effects of river discharge and seasonal winds on the shelf off southeastern South America. Continent. Shelf Res. 28, 1607–1624.

Moulin, M., Aslanian, D., Unternehr, P. 2010. A new starting point for the South and Equatorial Atlantic Ocean. Earth-Sci. Rev. 98, 1–37. doi:10.1016/j.earscirev.2009.08.001

Moulin, M., Aslanian, D., Rabineau, M., Patriat M., and Matias, L. 2012. Kinematic Keys of the Santos - Namibe Basins, In: Mohriak, W.U., Danforth, A., Post, P.J., Brown, D.E., Tari, G.C., Nemcok, M. and Sinha, S.T. (eds). Conjugate Divergent Margins. *Geological Society, London, Special Publications*, 369, http://dx.doi.org/10.1144/SP369.3.

Mudelsee, M., Stattegger, K. 1997. Exploring the structure of the mid-Pleistocene revolution with advanced methods of time-series analysis. Geol. Rundsch. 86, 499–511. doi:10.1007/s005310050157

Nagai, R.H., Ferreira, P.A.L., Mulkherjee, S., Martins, M.V., Figueira, R.C.L., Sousa, S.H.M., Mahiques, M.M., 2014. Hydrodynamic controls on the distribution of surface sediments from the southeast South American continental shelf between 23°S and 38°S. Continent. Shelf Res. 89, 51–60.

Nagender Nath, B., Sijinkumar, A. V., Borole, D. V., Gupta, S. M., Mergulhao, L. P., Mascarenhas-Pereira, M. B. L., Ramaswamy, V., Guptha, M. V. S., Possnert, G., Aldahan, A., Khadge, N. H. and Sharma, R. 2013. Record of carbonate preservation and the Mid-Brunhes climatic shift from a seamount top with low sedimentation rates in the Central Indian Basin. Boreas, Vol. 42, pp. 762–778. doi: 10.1111/j.1502-3885.2012.00304.x. ISSN 0300-9483.

Nürnberg, D., Müller, R.D. 1991. The tectonic evolution of the South Atlantic from Late Jurassic to present. Tectonophysics 191, 27–53. doi:10.1016/0040-1951(91)90231-G

Paillard, D., Labeyrie, L., Yiou, P. 1996. Macintosh Program performs time-series analysis. Eos Trans. Am. Geophys. Union 77, 379–379. doi:10.1029/96EO00259.

PAGES : Past Interglacials Working Group of PAGES. 2016. Interglacials of the last 800,000 years, Rev. Geophys., 54, 162–219, doi:10.1002/2015RG000482.

Park, K., Wang, R., Xiao, W., Polyak, L., Cho, H. G., and Khim, B. K. 2022. Increased terrigenous input from North America to the northern Mendeleev Ridge (western Arctic Ocean) since the mid-Brunhes Event. *Scientific reports*, *12*(1), 1-10.

Philander, S. G., 2008. Ed., Encyclopedia of global warming and climate change, vol. 2, 3 vols. Los Angeles: SAGE. pp. 519-522.

Piola, A.R., Matano, R.P., Palma, E.D., Möller, O.O., Campos, E.J.D. 2005. The influence of the Plata River discharge on the western South Atlantic shelf. Geophys. Res. Lett. 32.

Pinheiro-Moreira, J.L., Nalpas, T., Joseph, P., Guillocheau, F. 2001. Stratigraphie sismique de la marge éocène du Nord du bassin de Santos (Brésil) : relations plate-forme/ systèmes turbiditiques ; distorsion des séquences de dépôt. Comptes Rendus Académie Sci. - Ser. IIA - Earth Planet. Sci. 332, 491–498. doi:10.1016/S1251-8050(01)01562-2

Rabineau, M., Berné, S., Aslanian, D., Olivet, J.-L., Joseph, P., Guillocheau, F., Bourillet, J.-F., Ledrezen, E., Granjeon, D. 2005. Sedimentary sequences in the Gulf of Lion: A record of 100,000 years climatic cycles. Mar. Pet. Geol., The Gulf of Lions: an overview of recent studies within the French "Margins" Programme 22, 775–804. doi:10.1016/j.marpetgeo.2005.03.010

Rabineau, M., Berné, S., Olivet, J.L., Aslanian, D., Joseph, P., Guillocheau, F. 2006. Paleosea levels reconsidered from direct observation of paleoshoreline position during Glacial Maxima (for the last 500 000 yr) (Earth and Planetary Science Letters, Volume: 252 Issue: 1-2 Pages: 119-137 DOI: 10.1016/j.epsl.2006.09.033 Published: NOV 30 2006.

Rabinowitz, P.D., LaBrecque, J. 1979. The Mesozoic South Atlantic Ocean and evolution of its continental margins. J. Geophys. Res. Solid Earth 84, 5973–6002. doi:10.1029/JB084iB11p05973

Raynaud, D., Blunier, T., Ono, Y., Delmas, R.J. 2003. The Late Quaternary History of Atmospheric Trace Gases and Aerosols: Interactions Between Climate and Biogeochemical Cycles. In: Alverson, K.D., Pedersen, T.F., Bradley, R.S. (eds) Paleoclimate, Global Change and the Future. Global Change — The IGBP Series. P.12-31. Springer, Berlin, Heidelberg. https://doi.org/10.1007/978-3-642-55828-3_2

Reis, A.T., Maia, R.M.C., Silva, C.G., Rabineau, M., Guerra, J.V., Gorini, C., Ayres, A., Arantes-Oliveira, R., Benabdellouahed, M., Simões, I., Tardin, R. 2013. Origin of step-like and lobate seafloor features along the continental shelf off Rio de Janeiro State, Santos basin-Brazil. Geomorphology, Continental Shelf Drowned Landscapes (INQUA-CMP and IGCP-526) 203, 25–45. doi:10.1016/j.geomorph.2013.04.037

Reis, A. T., Amendola, G., Dadalto, T. P., Silva, C. G., Poço, R. G. T. C., Guerra, J.V., Martins, V., Rebouças, R. C., Gorini, C., Rabineau, M. 2020. Arquitetura e Evolução Deposicional da Sucessão Sedimentar Pleistoceno Tardio-Holoceno (últimos ~20 Ka) da Baía de Sepetiba (RJ).. Geociências (São Paulo. Online), v. 39, p. 695

Ridente, D., Trincardi, F., Piva, A., Asioli, A., Cattaneo, A. 2008. Sedimentary response to climate and sea level changes during the past ~400 ka from borehole PRAD1–2 (Adriatic margin). Geochem. Geophys. Geosystems 9, Q09R04. doi:10.1029/2007GC001783

Rodriguez-Suarez, C. 2005. Sea-bottom shear-wave velocities and mode conversions. Revista Brasileira de Geofisica 23(1): 75-87

Rothwell, R. G. (2006) New Techniques in Sediment Core Analysis https://doi.org/10.1144/GSL.SP.2006.267, Geological Society of London Publisher

Salgado, A.A.R., Rezende, E. de A., Bourlès, D., Braucher, R., da Silva, J.R., Garcia, R.A. 2016. Relief evolution of the Continental Rift of Southeast Brazil revealed by in situ-produced 10Be concentrations in river-borne sediments. J. South Am. Earth Sci. 67, 89–99. doi:10.1016/j.jsames.2016.02.002

Santos, T. P., Lessa, D. O., Venancio, I. M., Chiessi, C. M., Mulitza, S., Kuhnert, H., Govin, A., Machado, T., Costa, K. B., Toledo, F., Dias, B. B., Albuquerque, A. L. S. 2017. Prolonged warming of the Brazil Current precedes deglaciations. Earth and Planetary Science Letters, v. 463, p. 1-12.

Schattner, U., Mi de Mahiques, M. M (2020). Post-rift regional volcanism in southern Santos Basin and the uplift of the adjacent South American coastal range, Journal of South American Earth Sciences, Volume 104, https://doi.org/10.1016/j.jsames.2020.102855.

Schuur Duncan, C., Goff, J.A., Austin Jr., J.A., Fulthorpe, C.S. 2000. Tracking the last sea-level cycle: seafloor morphology and shallow stratigraphy of the latest Quaternary New Jersey middle continental shelf. Mar. Geol. 170, 395–421. doi:10.1016/S0025-3227(00)00082-7

Shackleton, N.J., Opdyke, N.D. 1973. Oxygen isotope and palaeomagnetic stratigraphy of Equatorial Pacific core V28-238: Oxygen isotope temperatures and ice volumes on a 105 year and 106 year scale. Quat. Res. 3, 39–55. doi:10.1016/0033-5894(73)90052-5

Shackleton, N.J., Berger, A., Peltier, W.R. 1990. An alternative astronomical calibration of the lower Pleistocene timescale based on ODP Site 677. Earth Environ. Sci. Trans. R. Soc. Edinb. 81, 251–261. doi:10.1017/S0263593300020782

Sibuet, J.-C., Hay, W.W., Prunier, A., Montadert, L., Hinz, K., Fritsch, J. 1984. Early evolution of the South Atlantic Ocean: role of the rifting episode. Initial Rep Deep Sea Drill Proj 75, 469–481.

Sierro, F. J., Andersen, N., Bassetti, M. A., Berné, S., Canals, M., Curtis, J. H., Dennielou, B., Flores, J.A., Frigola, J., Gonzalez-Mora, B., Grimalt, J.O., Hodell, D.A.., Jouet, G., Perez-Folgado, M., Schneider, R., 2009. Phase relationship between sea level and abrupt climate change, Quat.Sci.Rev.28 (25–26),p. 2867–2881.

Silveira, I. C. A., Schmidt, A. C. K., Campos, E. J. D., Godoi, S. S., Ikeda, Y. 2001. A Corrente do Brasil ao Largo do Sudeste Brasileiro. Revista Brasileira de Oceanografia, São Paulo, v. 48, n.2, p. 171-183

Smith, W., and Sandwell, D., 1997, Measured and Estimated Seafloor Topography, World Data Service for Geophysics, Boulder Research Publication.

Stramma, L., England, M. 1999. On the water masses and mean circulation of the South Atlantic Ocean. J. Geophys. Res. Oceans 104, 20863–20883. doi:10.1029/1999JC900139

Souza, R.B., Robinson, I.S., 2004. Lagrangian and satellite observations of the Brazilian Coastal Current. Continent. Shelf Res. 24, 241–262.

Tesson, M., Labaune, C., Gensous, B., Delhaye-Prat, V. 2010. Quaternary compound incised valleys of the Roussillon coast (SE France): correlation of seismic data with core data. Bull. Soc. Geol. Fr. 181, 183–196. doi:10.2113/gssgfbull.181.2.183

Toledo, F. A. L.; Cachao, M. ; Costa, K. B. 2007. Planktonic foraminifera, calcareous nannoplankton and ascidian variations during the last 25 kyr in the Southwestern Atlantic: a paleoproductivity signature?. Marine Micropaleontology, v. 64, p. 67-79.

Toledo, F. A.L.; Quadros, J. P.; Camillo, E.; Santarosa, A. C. A.; Flores, J.A.; Costa, K. B., 2016. Plankton biochronology for the last 772,000 years from the western South Atlantic Ocean. Marine Micropaleontology. , v.127, p.50 - 62.

Viana, A.R., Faugères, J.-C., Stow, D.A.V. 1998. Bottom-current-controlled sand deposits — a review of modern shallow- to deep-water environments. Sediment. Geol., Contourites, Turbidites and Process Interaction 115, 53–80. doi:10.1016/S0037-0738(97)00087-0

Wilson K. E., Maslin, M.A., Burns, S.J. 2011. Evidence for a prolonged retroflection of the North Brazil Current during glacial stages. Paleogeography, Paleoclimatology, Paleoecology 301 p. 86-96.

Yin, Q. Z., and Berger, A. 2010. Insolation and CO2 contribution to the interglacial climate before and after the Mid-Brunhes Event. *Nature Geoscience*, *3*(4), 243-246.

Zalan, P.V., de Oliveira, J.A.B. 2005. Origem e evolucao estrutural do sistema de riftes cenozoicos do sudeste do Brasil. Tecton. Evol. Cenozoic Rift Syst. SE Braz. 13, 269–300.

Zhuo, H., Wang, Y., Shi, H., He, M., Chen, W., Li, H., Wang, Y., Yan, W. 2015. Contrasting fluvial styles across the mid-Pleistocene climate transition in the northern shelf of the South China Sea: Evidence from 3D seismic data. Quat. Sci. Rev. 129, 128–146. doi:10.1016/j.quascirev.2015.10.012